

### Remarks

Further and favorable reconsideration is respectfully requested in view of the foregoing amendments and following remarks.

Thus, the amendments set forth above serve to limit the claimed subject matter to a methanol-reforming **method**, i.e. the claims to the catalyst have been cancelled or amended to recite the method.

More specifically, claim 2 has been amended to recite the method, and to depend from claim 21 which is directed to the method. Amended claim 2 thus corresponds to claim 20 directed to the method; and claim 20 has therefore been cancelled.

Claims 3 and 5 directed to the catalyst have been cancelled.

Claim 6 has been amended to recite the method and to depend from claim 23 which is directed to the method. Amended claim 6 thus corresponds to claim 24 which is directed to the method; and claim 24 has therefore been cancelled.

Claims 12-13, 15-16 and 18-19, all directed to the catalyst, have been cancelled.

Claim 21 has been rewritten in independent form, by incorporating the subject matter of claim 3 from which it depended.

Similarly, claim 23 has been rewritten in independent form by incorporating the subject matter of claim 5 from which it depended.

Claim 26 has been amended to recite the method, and to depend on method claim 23.

Applicants respectfully submit that the foregoing amendments should be entered, even though they are being presented after a final rejection. As indicated above, Applicants are no longer claiming the catalyst itself, but only a method of using the catalyst in a methanol-reforming reaction. The amendments also serve to render many of the rejections set forth by the Examiner moot. Furthermore, the Examiner has already considered the method claims, and therefore, entry of the amendments will not require any further consideration and/or search of the prior art. In view of these circumstances, Applicants take the position that the amendments should be entered.

The patentability of the presently claimed invention after entry of the foregoing amendments, over the disclosures of the references relied upon by the Examiner in rejecting the claims, will be apparent upon consideration of the following remarks.

As indicated above, the amendments serve to render many of the prior art rejections moot. These are the rejection of claims 2-3 on page 2 of the Office Action, the rejection of claims 12-13 on page 3, the rejection of claims 15-16 on page 4, the rejection of claims 5-6, 12-13 and 26 on page 8 and the rejection of claims 18-19 on page 9 of the Office Action.

The rejection of claims 20-21 under 35 U.S.C. §103(a) as being unpatentable over Shaw et al. (US '701) in view of Takuya et al. (JP '402) as evidenced by Lessing (US '655) is respectfully traversed.

Shaw et al. teach an intermetallic  $\text{Ni}_3\text{Al}$ , but do not teach producing hydrogen.

Takuya et al. teach a Ni-containing metal deposited on an Al-containing metallic member to form a catalyst on the surface for methanol steam reforming or methanol decomposition. However, this reference does not teach that  $\text{Ni}_3\text{Al}$  can be used as a catalyst for methanol steam reforming or methanol decomposition. Actually, Takuya et al. disclose that the above-mentioned Ni-containing metal being deposited on the metallic member is an alloy of Ni and Cu or Ni and Zn (page 6, lines 13-16 in right column). There is no disclosure of a catalyst of Ni-Al alloy.

Lessing shows "NiAl or  $\text{Ni}_3\text{Al}$  which can catalyze steam reforming of hydrocarbons" in the Abstract. However, there is no example or evidence of such catalytic properties of NiAl and  $\text{Ni}_3\text{Al}$  in this reference.

The following comments will make reference to the attached Fig. 1 (Al-Ni phase diagram), as well as the following references, copies of which are submitted herewith:

- [1] J. Freei, W.J.M. Pieters, R.B. Anderson, *Journal of Catalysis* 16 (1970) 281-291 (see the introduction part on p. 281).
- [2] S. Tanaka, N. Hirose, T. Tanaki, Y.H. Pgata, *Journal of The Electrochemical Society* 147 (2000) 2242-2245.
- [3] Ya Xu, S. Kameoka, K. Kishida, M. Demura, A.P. Tsai, T. Hirano, Catalytic properties of  $\text{Ni}_3\text{Al}$  intermetallics for methanol decomposition, *Materials Transactions* 45 (2004) 3177-3179.
- [4] Ya Xu, Satoshi Kameoka, Kyosuke Kishida, Masahiko Demura, An-pang Tsai, Toshiyuki Hirano, *Intermetallics* 13 (2005) 151-155.
- [5] D.H. Chun, Ya Xu, M. Demura, K. Kishida, M.H. Oh, T. Hirano, D.M. Wee, Spontaneous catalytic activation of  $\text{Ni}_3\text{Al}$  thin foils in methanol decomposition, *Journal of Catalysis* 243 (2006) 99-107.

In a Ni-Al system there are four stable intermetallic compounds,  $\text{NiAl}_3$ ,  $\text{Ni}_2\text{Al}_3$ ,  $\text{NiAl}$  and  $\text{Ni}_3\text{Al}$  (see the attached Fig. 1 Al-Ni phase diagram). Among them a mixture of  $\text{NiAl}_3$  and  $\text{Ni}_2\text{Al}_3$  is used as a precursor alloy for catalysts (usually called Raney Ni catalysts). The commercial precursor alloy from which the Raney Ni catalysts are produced usually contains around 50 wt. % Ni and 50 wt. % Al. The Raney Ni catalysts are produced from the precursor alloy by leaching Al in a NaOH solution. **For  $\text{NiAl}$  and  $\text{Ni}_3\text{Al}$ , it was common knowledge that a lower catalytic activity can be expected because it is difficult to effectively leach Al from  $\text{NiAl}$  and  $\text{Ni}_3\text{Al}$  [Refs. 1-2].** For example, in Ref. 2, Tanaka et al. prepared Raney-Ni cathodes by leaching Al from various previous Ni-Al alloys ( $\text{NiAl}_3$ ,  $\text{Ni}_2\text{Al}_3$ ,  $\text{NiAl}$  and  $\text{Ni}_3\text{Al}$ ). They found that **an active Raney-Ni electrode was obtained only from Al rich alloys ( $\text{NiAl}_3$  and  $\text{Ni}_2\text{Al}_3$ )** because the dissolution of Al from these alloys proceeded in NaOH solution.

In the present invention, Applicants for the first time examined the catalytic activity of single-phase  $\text{Ni}_3\text{Al}$  for hydrogen production from methanol, and found that alkali-leached  $\text{Ni}_3\text{Al}$  shows a high activity for methanol decomposition [Refs. 3-5].

In rejecting claims 20-21, the Examiner takes the position that it would have been obvious to utilize the method of producing hydrogen of Takuya et al. with the compound of Shaw et al. in order to increase the reforming reaction rate for methanol and further, as Lessing teaches the  $\text{Ni}_3\text{Al}$  intermetallic material being used as a catalyst for methane reformation, "it would have been obvious to one of ordinary skill in the art at the time of the invention to utilize a similar material for a similar purpose." However, in view of the foregoing comments concerning attached Fig. 1 and References 1-5, Applicants respectfully submit that the Examiner is mistaken in taking the position that it would have been obvious to utilize a similar material for a similar purpose. That is, concerning References 1-2, the art-skilled would have been led away from using  $\text{Ni}_3\text{Al}$  in a methanol reforming reaction as in the present invention; and the art-skilled would certainly not have expected the high activity for  $\text{Ni}_3\text{Al}$  in this reaction as shown by References 3-5.

Thus, Applicants take the position that the references do not establish a presumption of obviousness, nor do the references suggest the high activity achieved by the present invention.

The rejection of claim 9 under 35 U.S.C. §103(a) as being unpatentable over Shaw et al., Takuya et al. and Lessing further in view of Fukui et al. (US '439) is respectfully traversed.

The comments set forth above concerning the Shaw et al., Takuya et al. and Lessing references are equally applicable to the rejection of claim 9, which is dependent on claim 21, which has been discussed above. Therefore, the rejection of claim 9 should be withdrawn for the same reason that the rejection of claim 21 should be withdrawn.

The rejection of claims 23-24 under 35 U.S.C. §103(a) as being unpatentable over Shaw et al. as modified by Lashmore et al. (US '431) as evidenced by Coll et al. (US '226) further in view of Takuya et al. is respectfully traversed.

The comments set forth above concerning the Shaw et al. and Takuya et al. references are equally applicable to this rejection. The Examiner's position is that it would have been obvious to use the  $\text{Ni}_3\text{Al}$  intermetallic compound of Shaw et al. (with the carbon nanofibers of Lashmore et al.) in the Takuya et al. method. However, as discussed above, and as supported by References 1-5 submitted herewith, the art-skilled would have been led away from using the intermetallic  $\text{Ni}_3\text{Al}$  compound of Shaw et al. in the method of Takuya et al. because of its poor catalytic activity, nor would the art-skilled have expected the superior results achieved in accordance with the present invention, particularly as shown by References 3-5.

The rejection of claim 27 under 35 U.S.C. §103(a) as being unpatentable over Shaw et al., Lashmore et al., Coll et al. and further in view of Fukui et al. is respectfully traversed.


Claim 27 is dependent on claim 23, which has been discussed above. Applicants take the position that claim 27 is patentable for the same reasons that claim 23 is patentable.

For these reasons, Applicants respectfully submit that the presently claimed invention is clearly patentable over the applied references.

Therefore, in view of the foregoing amendments and remarks, it is submitted that each of the grounds of rejection set forth by the Examiner has been overcome, and that the application is in condition for allowance. Such allowance is solicited.

Respectfully submitted,

Ya XU et al.

By   
Michael R. Davis  
Registration No. 25,134  
Attorney for Applicants

MRD/pth  
Washington, D.C. 20005-1503  
Telephone (202) 721-8200  
Facsimile (202) 721-8250  
February 5, 2010

# EXHIBIT

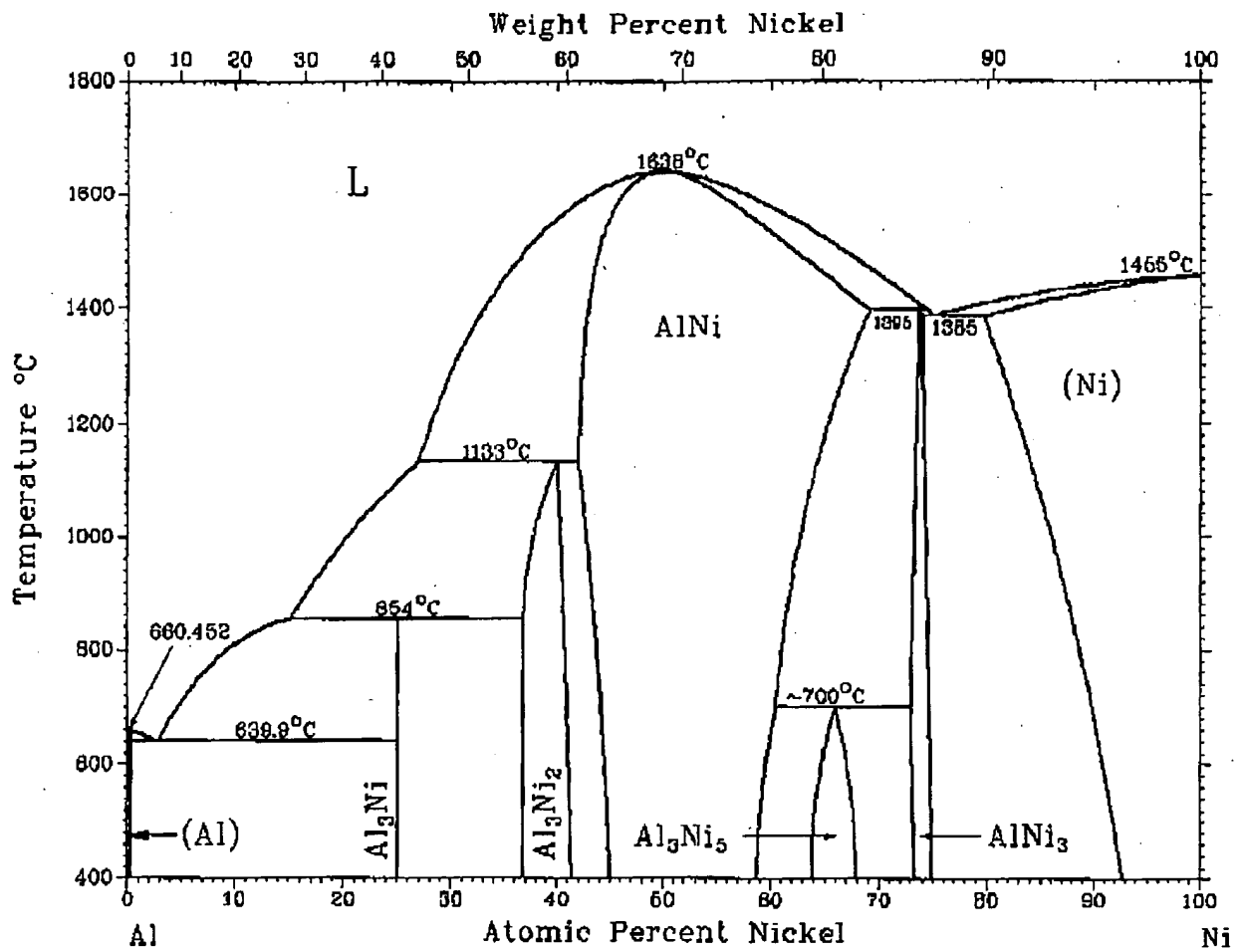


Fig. 1 Al-Ni phase diagram

## The Structure of Raney Nickel

### II. Electron Microprobe Studies

J. FREEL, W. J. M. PIETERS, AND R. B. ANDERSON

*Department of Chemical Engineering, McMaster University, Hamilton, Ontario*

Received June 2, 1969

The activation of Raney nickel alloys containing 42 and 50 wt % Ni by reaction with aqueous sodium hydroxide was studied by metallographic methods including an electron probe microanalyzer. The alloys contained a eutectic of about 5 wt % Ni,  $\beta$ (NiAl), and  $\gamma$ (Ni<sub>3</sub>Al) phases; NiAl was not found in these alloys. For any phase the attack by alkali advances as a front yielding a sharp gradient between alloy and activated catalyst, or, in the case of eutectic, a void. In activated catalysts portions originating from  $\beta$  and  $\gamma$  alloys can be recognized on the basis of structural characteristics. The activated materials contain what appears to be shrinkage cracks, which are larger and more numerous in catalyst derived from  $\beta$ - rather than  $\gamma$ -phase. In moderately concentrated aqueous alkali, the eutectic and  $\beta$  phase react more rapidly than  $\gamma$  phase. For example, in a 10-min leaching of 20-50 mesh alloy at 50°C in which half of the aluminum was oxidized, the product contained activated  $\beta$ -phase and  $\gamma$  alloy. In dilute alkali the attack on the alloy was non-selective and the catalyst contained substantial amounts of alumina. Our data indicate that analyses of moderate accuracy can be obtained on the porous activated Raney nickel by the electron probe microanalyzer.

#### INTRODUCTION

In the preparation (1) of Raney nickel, a large part of the aluminum is converted to sodium aluminate, most of which is removed in subsequent water washing. The starting Raney alloys normally contain 40 to 50 wt % nickel. Alloys of higher nickel content usually contain significant amounts of the compound NiAl, which does not react with alkali (2), while alloys containing less nickel yield correspondingly less catalyst. Alloys in the composition range of 40-50 wt % nickel are not homogeneous, but may contain several phases (3). The structure of the initial alloys and their reactivity toward alkali is therefore an interesting feature of the Raney catalyst.

Various authors have investigated aspects of this problem. Littman and Bliss (4) described optical micrographs of commercially extracted catalyst in which two distinct areas could be observed and suggested that these might be related to the

phases present in the original alloy. Mason (5) demonstrated this retention of the alloy appearance more clearly. The effect of alloy structure on catalytic activity of the extracted catalyst has also been examined (2, 6). However, several anomalies still remain; for example, different authors have reported that NiAl is (2) and is not (6) more reactive toward alkali than Ni<sub>3</sub>Al.

In the present study, we used the techniques of optical metallography to examine the microstructure of commercial Raney alloys and their reaction with sodium hydroxide to form Raney nickel. The interpretation of optical appearance was greatly facilitated by the use of an electron probe microanalyzer. Apparently analytical data of moderate accuracy can be obtained for the porous catalysts.

#### EXPERIMENTAL METHODS

Two large batches of commercial Raney alloy, nominally of 42 and 50 wt % nickel

composition [alloys A and B of Part I (7)] were used throughout.

Standard metallographic procedures were used in mounting and polishing specimens. Raney alloys were mounted in bakelite. Fully and partly extracted catalysts were pyrophoric, and were stored in ethanol to prevent oxidation. These samples were placed in glass moulds together with ethanol. A liquid, cold-mounting resin was added when most of the ethanol had evaporated. Polishing appeared to inhibit atmospheric oxidation substantially. The prepared surface was stable for several hours in terms of optical appearance, after which discoloration and surface pitting could be observed. Samples allowed to oxidize vigorously in air prior to mounting had a uniform, strongly reflecting surface devoid of the optical features of the normal catalyst.

An "Acton" electron probe microanalyzer (fixed angle of takeoff =  $18^\circ$ ) was used at a beam voltage of 25 kV and specimen current 50 nA unless otherwise stated. Quartz and mica diffraction crystals were used to obtain the nickel and aluminum  $K\alpha$  lines, respectively.

Good conduction of electrons away from the probe impact area is essential to avoid overheating or "hot spot" formation. Specimens were found to be sufficiently conducting after vacuum deposition of a layer of carbon about 1000 Å thick.

Samples of several nickel-aluminum intermetallic compounds, kindly furnished by Professor G. R. Purdy of this University, were used in preparing calibration curves for nickel and aluminum, as given in Fig. 1. The standard alloys were prepared by repeated nonconsumable-electrode arc melting in argon. The samples were weighed before and after melting and the alloys were checked metallographically for homogeneity.

## RESULTS

### 1. The Structure of Commercial Raney Alloys

Possible phases for nickel-aluminum alloys containing 40-50 wt % nickel, taken from the phase diagram of Alexander and Vaughan (8), are given in Table 1. These

TABLE 1  
POSSIBLE PHASES FOR NICKEL-ALUMINUM ALLOYS  
CONTAINING 40-50 WT % NICKEL

Phase	Symbol	Nickel content (wt %)
Solid solutions of Ni in Al(1)	$\alpha$	0.05 or less
I + NiAl <sub>3</sub>	Eutectic	~5
NiAl <sub>3</sub>	$\beta$	42
Ni <sub>2</sub> Al <sub>3</sub>	$\gamma$	56-60
NiAl	$\delta$	80-83

phases have been designated in different ways, and we have used the symbols in Table 1, to remain consistent with the work of Mason (6), which is most pertinent to the present study. Eutectic, NiAl<sub>3</sub> and Ni<sub>2</sub>Al<sub>3</sub> may be clearly distinguished in an unetched, polished surface of such alloys (see Fig. 3A). Etchants are required (8) to reveal the compound NiAl, but none was detected in the present study either by etchants or by electron probe microanalysis of  $\gamma$ -phase grains.

The 42 and 50 wt % nickel alloys, received as irregular chips about  $\frac{1}{4}$  cm<sup>3</sup> in volume, were crushed mechanically and screened in U. S. Standard sieves. For both alloys, six mounts, each containing some thirty 30-50 mesh pieces, were examined optically. Volume concentrations of  $\gamma$ ,  $\beta$ , and eutectic phases in the two alloys, calculated by standard metallographic methods (8), are given in Table 2. For each of the alloys the amounts of the phases varied moderately. Pieces of 50/50 alloy, for example, contained from 54 to 66 vol %  $\gamma$ , those of 42/58 from 25 to 50%. However, all pieces of the former examined contained little eutectic, all of the latter, substantial amounts. The aluminum-rich alloy (42/58) contained significantly less  $\gamma$ -phase than the (50/50) alloy.

TABLE 2  
PHASE ANALYSIS OF RANEY NICKEL ALLOYS

Sample alloy	$\gamma$ (av vol %)	$\beta$ (av vol %)	Eutectic (av vol %)
A 50/50	58	40	~2
B 42/58	30	45	25



CALIBRATION	FOR	BINARY
NICKEL-ALUMINUM	SERIES	

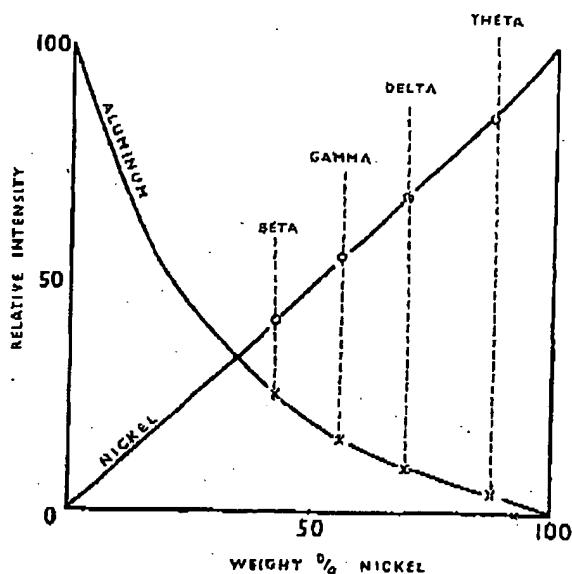


Fig. 1. Electron probe calibration for nickel-aluminum system at 25 kV.

Typical micrographs of 30-50 mesh pieces of the alloys are given in Figure 3B and C. As reported previously (6),  $\gamma$ -phase grains in 50/50 alloy were significantly larger than those in 42/58. The smaller grains of  $\text{Ni}_3\text{Al}$  in the 42/58 alloy often showed typical dendritic structure.

The composition of these phases was confirmed by electron probe microanalysis.

The aluminum-rich/nickel-deficient nature of the eutectic precipitate is illustrated in the probe scans shown in Fig. 4. Figure 4A is an oscilloscope display of the specimen current from a region containing  $\beta$  and eutectic only, the eutectic appearing as bright areas, and Figure 4B and C are records of the aluminum and nickel  $K\alpha$  yields, respectively.

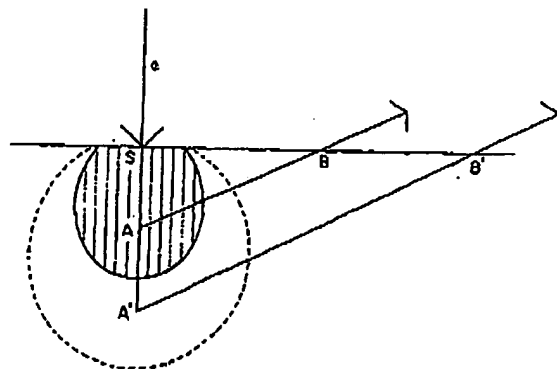


Fig. 2. Schematic representation of X-radiation in the same solid in microporous and nonporous form.

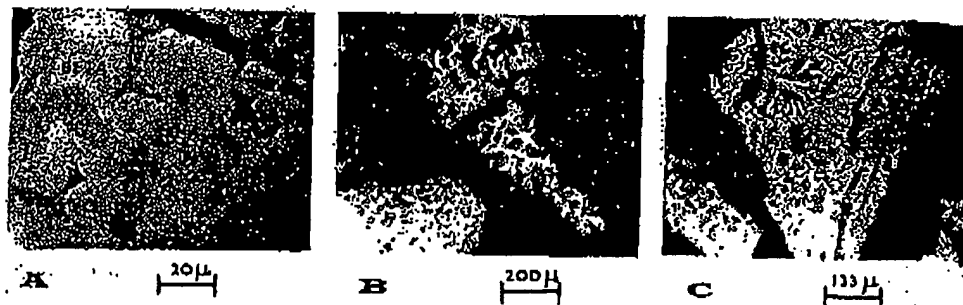


FIG. 3. (A and C) are optical micrographs of the 42 wt % nickel alloy B, containing  $\beta$ - and  $\gamma$ -eutectic phases. A micrograph of the 50 wt % nickel alloy A, containing only dark colored  $\gamma$ -phase grains in a matrix of the lighter colored  $\beta$ -phase, is given in (B).

## 2. The Reaction of Raney Alloys with Sodium Hydroxide

The reactivity of the polished alloy surface to sodium hydroxide has been studied (5). The order of reactivity found was:



We have repeated such experiments, etching 42/58 alloy with 20% aqueous NaOH at room temperature, since this material contains all three constituent phases. Under these conditions eutectic and  $\beta$ -phase react rapidly, while  $\gamma$ -phase apparently did not begin to react for 25 min at which time brown discoloration could

be observed. The  $\gamma$ -phase was therefore much the least reactive and the removal of eutectic (95 wt % Al) to leave voids was rapid. We could not, however, distinguish between the rates of reaction of  $\beta$  phase and eutectic. For example, immersion for 1 min darkens  $\beta$ -phase sufficiently to reverse the contrast between  $\beta$  and  $\gamma$ , at which time the eutectic precipitate is apparently unreacted. After 4 min, many areas of  $\beta$ -phase begin to show surface pitting, again at a time when reaction of eutectic is small. Prolonged etching (15 min), not yet sufficient to cause reaction of  $\gamma$ , results in the appearance of microcracks

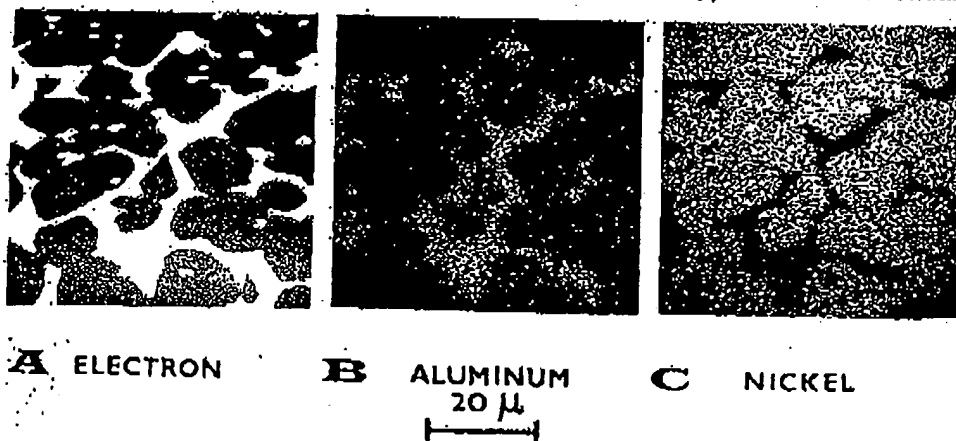


FIG. 4. Microprobe scans of an area of surface of alloy B which contained only the eutectic and  $\beta$ -phase. The eutectic precipitate, having a lower average atomic weight, reflects fewer electrons and consequently is light in color in records of specimen current (A). The higher aluminum content, and therefore nickel deficiency, of the eutectic is illustrated by the aluminum and nickel  $K\alpha$  scans in (B and C).



FIG. 5. Optical micrographs of alloy A after reaction with concentrated aqueous sodium hydroxide. The interface between reacted and unreacted alloy in a cross-sectional sample (see text for details) is shown in (A), where the unreacted areas within the product zone were found to be  $\gamma$ -phase. Similar areas of unreacted  $\gamma$ -phase (lightest in color) are shown in more detail in (B). A typical micrograph of the structure observed after 10-min reaction of 80-50 mesh alloy A is given in (C); the white areas were unreacted  $\gamma$ -phase.

in the  $\beta$ -phase, concurrent with the formation of voids formerly occupied by eutectic. A similar broken structure of reacted  $\beta$ -phase is shown in the micrographs of Mason (5). We believe these microcracks were too irregular to be associated with subgrain structure and suggest that they are in fact shrinkage voids due to the volume contraction accompanying aluminum removal. In support of this conclusion, it may be noted that similar cracks were observed in reacted  $\gamma$  but were more prevalent in reacted  $\beta$ -phase which would be expected to undergo larger volume changes. The possibility that such phenomena are due to the etching of cold-working faults

induced during polishing is considered unlikely, since similar features are encountered at appreciable depth in sectioned samples (see Fig. 5B) and in micrographs of the completely extracted catalyst (Fig. 6A and B).

The depth to which reaction of  $\beta$ -phase penetrates before attack occurs on  $\gamma$ -phase was then investigated by examining a polished section perpendicular to the original direction of caustic attack. The 50/50 alloy was used because of its low concentration of eutectic and larger  $\gamma$  grains. Polished alloy surfaces were reacted for various times in 20% NaOH at 50°C, washed in water and ethanol, capped with

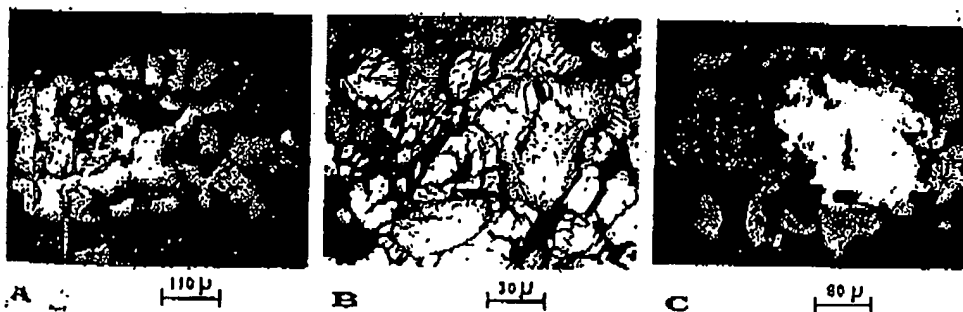


FIG. 6. The structures of 30-50 mesh pieces of 50 wt. % nickel alloy A after prolonged extraction at 50 and 107°C in 20% aqueous NaOH are shown in (A and B), respectively. In (A), catalyst originating from the former  $\gamma$ -phase grains is lighter in color than that from  $\beta$ -phase, while the reverse is true in (B). The small white areas in (A) are unreacted  $\gamma$ -phase. The structure shown in (C) is typical of that found for samples extracted by the IOT method. No preferential reaction amongst the alloy phases is observed; partly reacted alloy pieces contain an unreacted core of all phases, surrounded by extracted catalyst.

mounting resin, sectioned perpendicular to the original surface plane, and the newly cut face was polished. In contrast to the lightly etched samples discussed above, penetration of several microns was required in order to examine the reaction interface, and the surface was pyrophoric. The reacted surface was therefore "capped" with cold mount just prior to complete solvent evaporation and the required cross-section was obtained on a coarse silicon carbide paper under water. Normal polishing procedures could then be followed.

Reacted and unreacted alloy could be distinguished, and the reaction of  $\beta$  proceeded to an average depth of some 60  $\mu$  before  $\gamma$ -phase began to react. Preferential reaction was still evident after much longer periods of reaction, the "product scale" containing unreacted  $\gamma$ -phase (Plate 3A). A higher magnification view of some of these partly reacted  $\gamma$  grains is given in Fig. 5B. The presence of an unreacted core surrounded by extracted catalyst may be seen in such grains.

Electron probe studies of these samples confirmed the conclusions based on optical appearance. For example, the bright, apparently unreacted regions in the product scale gave identical nickel and aluminum counting rates to those obtained from  $\gamma$ -phase. The darker, reacted regions gave data quantitatively similar to those obtained with completely extracted catalyst. It may also be noted, that to the scale of probe resolution, no variation in aluminum concentration could be observed on approaching the reaction interface from either the reacted (Raney nickel) or unreacted ( $\beta$  or  $\gamma$  alloy) sides.

It must be emphasized that a degree of subjective judgment is required in reaching these conclusions. The impact area of the electron beam is observed optically and the nature of the volume analyzed is assigned in this way. However, the element of volume analyzed is not always of the same structure as the area of surface thus viewed. Occasional contradictory data, statistically outweighed by "normal" readings, were therefore ascribed to regions where a different phase or a hole just

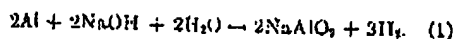
beneath the surface had contributed to the analysis but was not visible optically.

Frequently, this assumption could be supported by other data. Holes, for example, could often be detected by probe scanning and oscilloscope display, giving lowered intensity in both nickel and aluminum  $K\alpha$ , relative to surrounding areas. Subsurface structures different from the visible probe impact area (e.g., a  $\gamma$ -phase grain perhaps 0.25  $\mu$  below an area identified optically as reacted  $\beta$  phase), are more difficult to prove, but may show up in displaying the specimen current variations from the region.

Assuming 30-50-mesh alloy pieces to be spheres of similar dimensions to the openings in a 30-mesh sieve (radius 0.03 cm) and that the reaction of such spheres with sodium hydroxide may be related to the planar etching reaction described above, the degree to which  $\beta$ -phase may react preferentially in a standard extraction process can be estimated. Such calculations suggest that all accessible  $\beta$ -phase in the powdered alloy will be converted to Raney nickel in about 10 min. (compared to about 100 min for complete reaction), and that  $\gamma$ -phase will be little reacted in this period. To test this postulate 6 g of 30-50 mesh, 50/50 alloy were added to 200 ml of 20% NaOH at 50°C. The reaction was carried out in a well stirred glass reactor (7) and hydrogen evolution was measured by a wet-test meter. After 10 min extraction, polished samples of the partly reacted solid had a structure typified by that shown in Fig. 5C. Electron probe analysis showed that the bright areas were unreacted  $\gamma$ -phase, the darker, reacted regions, apparently Raney nickel. After 90-min reaction, most pieces contained no unreacted alloy. An occasional larger piece did contain a little unreacted  $\gamma$ -phase and micrograph 6A shows one such piece, in which the three small white areas were identified as  $\text{Ni}_3\text{Al}$ . The contrast between other areas in this micrograph is between reacted  $\gamma$  and reacted  $\beta$ , the former being somewhat lighter in color. This assignment was demonstrated more clearly by aluminum extraction from pieces of 42/58 ingot

in which the  $\gamma$ -phase had a markedly dendritic appearance. This "memory" of the grain structure of the original alloy was stable thermally, 24-hr evacuation at 450°C producing no visible change. The catalyst particles have low mechanical strength, however, slight stress being sufficient to grind the material.

The hydrogen evolved in a 10-min extraction corresponded to about 50% of complete reaction assuming the stoichiometric reaction:



The rate of reaction, deceleratory throughout, decreased markedly after 10 min. The hydrogen evolved after 90 min was 90% of that required by Eq. (1). These values are consistent with the metallographic data.

Littman and Bliss (4) observed two distinct areas in optical micrographs of activated commercial Raney nickel, and suggested that the different areas may have been derived from different nickel-aluminum alloys. In their published micrographs (4), areas derived from the  $\beta$ - and  $\gamma$ -phases can be identified; however, the contrast is the reverse of that shown in Figure 6A for a catalyst activated at 50°C. We have observed the same reversal of contrast for catalysts prepared under more severe conditions, e.g., Raney nickel prepared by reaction in boiling 20% alkali for 2 hr [cf. catalyst IIIA<sub>2</sub> in Part I (7)] shown in Fig. 6B.

Mason (5) found equal reactivities for the  $\gamma$ - and  $\beta$ -phases of Raney alloys to aqueous alkali; both metallographic and X-ray diffraction studies showed unreacted  $\gamma$  and  $\beta$  alloys coexistent in catalyst particles. However, these catalysts prepared at the Institute for Gas Technology (IGT) were activated with substantially less than the stoichiometric amount of NaOH required for Eq. (1). We have prepared catalysts by a similar method [Type IV catalysts of Part I (7)]. In one such preparation, 30 ml of 20% NaOH (about 1/4 of the requirements of Eq. (1)) were added to 40 g of 50-100 mesh, 50/50 alloy in 300 ml of distilled water at 80°C. An initially rapid reaction soon subsided and was followed by

a short induction period, after which rapid hydrogen evolution recommenced. Reaction was stopped when the evolved hydrogen corresponded to 80% of that predicted for complete aluminum oxidation. The solid was washed to neutrality in distilled water, large flocks of alumina being evident in the decanted layers. A typical micrograph of this material is given in Fig. 6C. Reacted and unreacted alloy may be clearly distinguished and both  $\gamma$  and  $\beta$  alloys are present in the unreacted core of the particle as demonstrated by Mason (5). Contrast between reacted  $\gamma$  and  $\beta$ , reported by Mason, is again observed, and it may be noted that such contrast is much more clearly defined in this type of preparation.

#### Quantitative Electron Probe Microanalysis

Electron probe microanalysis was used to examine two problems defined by the preceding optical studies: (i) Did the retention of grain structure between alloy and catalyst and the optical contrast between catalyst derived from NiAl<sub>3</sub> and from Ni<sub>2</sub>Al<sub>3</sub> correspond to a difference in chemical composition? (ii) To the spatial resolution of microprobe analysis, perhaps 1  $\mu^2$  under favorable circumstances, were areas of similar optical appearance also areas of the same chemical composition?

Experimental data were obtained largely at 25 kV beam voltage 50 nA specimen current. Since operating voltage is normally chosen to be about three times the critical excitation voltage for the element and X-ray line desired, the operating voltage was optimized for nickel analyses for the most part. For materials of low aluminum content, aluminum  $K\alpha$  intensities were very small under these conditions (Fig. 1) and aluminum analyses consequently of lower accuracy. Additional data were obtained at 11.5 kV, 20 nA for such catalysts. Aluminum  $K\alpha$  intensities were then appreciably larger relative to pure aluminum and more accurate calibrations could be obtained at low aluminum concentration.

Standard counting techniques were used to examine several catalyst preparations in detail. Six particles of each preparation were studied and about 30 point counts

TABLE 3  
 MICROPHONE ANALYSES FOR A VARIETY OF RANEY CATALYSTS

Catalyst type	Region analysed	25 kV		11.5 kV		Chemical analysis	
		Ni (%)	Al (%)	Ni (%)	Al (%)	Ni (wt %)	Al (wt %)
1. Prepared at 50°C [types IA, IIA, and IIB of Ref. (7)]	$\gamma$ -derived	70	10	78	6	81	8.2
	$\beta$ -derived	70	6	70	3		
2. Data from interface of etched (50/50) alloy of sectioned type	$\gamma$ -derived	82	10				
	$\beta$ -derived	82	5				
3. Prepared at 107°C [type IIIA of Ref. (7)]	$\gamma$ -derived	82	3	84	2.5	86	5.2
	$\beta$ -derived	86	1.5	88	1		
4. IGT Type from 50/50 alloy [type IV of Ref. (7)]	$\gamma$ -derived	50	16			40	22
	$\beta$ -derived	44	17				

were taken from different regions of each particle. For each point count, sufficient data were obtained to ensure reasonable statistical accuracy. Nickel and aluminum X-ray intensities were first expressed as a fraction of the intensities for pure nickel and aluminum and then corrected using the calibration curve of Fig. 1, or the corresponding calibration at 11.5 kV. All results for any particular catalyst were then averaged over the region analyzed, i.e., area that had originated from  $\gamma$  or  $\beta$  alloy. Data of this type, together with the relevant nickel and total aluminum analyses obtained by chemical methods are given in Table 3. Details of the results obtained may be summarized thus:

(i) For any given catalyst of types I, II, and III (7), nickel intensities were relatively constant ( $\pm 5\%$ ) from one point to another in either the regions derived from  $\beta$  alloy or those derived from  $\gamma$  alloy. Similar data for different catalysts prepared in the same way was only slightly less reproducible (mean deviation  $\pm 7\%$ ), and all catalysts of types I and II gave equivalent results within these limits. Data were less reproducible ( $\pm 15\%$ ) for the type IV (IGT) catalyst and only in this case was significant variation in nickel content between the  $\gamma$ - and  $\beta$ -derived regions noted.

(ii) In general, aluminum analyses

showed greater variation (mean deviation  $\pm 20\%$ ) in optically similar regions. For all except the type IV catalyst, however, the average of such values from one particle to the next was always relatively reproducible ( $\pm 5\%$ ) and marked variation in the aluminum content of the two catalyst regions was always observed (Table III). Averaged values for the type IV catalyst were also reproducible to  $\pm 5\%$ , but no systematic variation between aluminum analyses for  $\beta$ - and  $\gamma$ -derived regions of the catalyst was observed.

To the scale of probe resolution, therefore, the chemical composition of types I, II, and III catalysts appears to be homogeneous in optically similar regions. However, those regions of catalyst formed from the  $\text{Ni}_3\text{Al}_2$  grains of the original alloy contain approximately twice as much aluminum and/or alumina as regions formed from  $\text{NiAl}_3$ . This is not observed in the type IV catalyst. However, the large quantities of alumina trihydrate present in this catalyst, apparently unevenly distributed, may mask a similar difference in the amount of aluminum yet unreacted. Both nickel and aluminum analyses were in acceptable agreement with the chemical data, even in the case of the type IV catalyst, estimated (7) to contain about 42 wt %  $\beta$   $\text{Al}_2\text{O}_3 \cdot 3\text{H}_2\text{O}$ .

The present data therefore suggest that

standard electron probe techniques yield analyses of moderate accuracy when applied to microporous materials. This result may best be understood by considering the characteristic X-radiation obtained from any nonporous solid and from the same solid in microporous form such that pore size is very small compared to probe resolution. In neither case will the whole of the incident electron flux generate X-rays. A certain fraction, determined largely by atomic number and surface topography, will be back-scattered with little loss of energy, but this quantity would not be expected to vary significantly between the porous and nonporous case. For the nonporous solid, the volume in which characteristic X-radiation is generated may be represented by the shaded area of Fig. 2. Schematically, an electron may be considered to penetrate to a depth  $SA$  and emerging X-ray quanta must pass through a distance  $AB$  in the solid en route to the spectrometer. For the microporous element, the volume analyzed (broken line) will be larger, the same electron may penetrate to a depth  $SA'$  and the emerging X-ray quanta must pass through a distance  $A'B'$  in the specimen.

However, to a first approximation, the volume analyzed will contain the same mass in either case. Thus an electron moving between  $S$  and  $A$  will encounter the same weight of solid as that moving along  $SA'$  and will generate the same amount of X-radiation. Further, since all distances within the specimen are small relative to the distance between specimen and spectrometer,  $AB$  and  $A'B'$  will be approximately parallel and emergent X-ray quanta will also encounter equivalent mass and undergo similar absorption processes. These relationships are shown by equations for electron penetration and X-ray emission and for X-ray absorption, which are functions only of mass-distance (12).

Clearly, these arguments would not be true for a material containing pores of a size similar to probe resolution. It may be noted, however, that mean pore diameters for the nickel catalysts used in the present work were about 30–60 Å (7).

## DISCUSSION

Samples of commercial 42 and 50 wt % nickel alloys were found to contain the same three phases;  $Ni_3Al$ ,  $NiAl$ , and a eutectic precipitate.  $NiAl$  was not detected in this batch of 50/50 alloy, although it has been observed (8) in other alloys of this composition. The 50/50 alloy contained a little more  $Ni_3Al$  and substantially less eutectic phase than the 42/58 material.

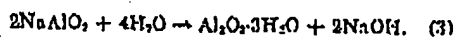
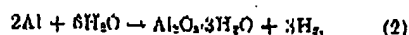
One cannot assume similar structural differences between all 42/58 and 50/50 alloys. It is clear from the phase diagram (5) that the method of cooling will greatly influence the microstructure. However, it seems reasonable to conclude that the differences observed would be predicted from the phase diagram for quenched alloys and might be anticipated on a more general basis for alloys prepared by rapid cooling of a well-mixed melt.

The fundamental difference in microstructure of the two alloys studied was the appearance of much of the additional aluminum content of the 42/58 material as eutectic precipitate. This eutectic phase, for which an average nickel content of about 5 wt % has been confirmed, must not be expected to contribute significantly to the final nickel catalyst. Thus, during reaction with sodium hydroxide, regions of eutectic precipitate were largely dissolved to leave voids in the alloy particles. In contrast, the residue after aluminum removal from both  $NiAl_3$  and  $Ni_3Al$  retained much of the appearance of the starting alloy since optical contrast between distinctive areas of the polished catalyst could be related to the original  $NiAl_3/Ni_3Al$  grain structure. Electron microprobe analyses further showed that Raney catalyst originating from  $Ni_3Al$  contained about twice as much aluminum and/or alumina as that originating from  $NiAl_3$ . This was true of catalysts prepared at 50°C (Fig. 6A) and also of those prepared in boiling alkali (Fig. 6B) when the previous optical contrast between  $\gamma$ -derived and  $\beta$ -derived catalyst was reversed and the overall aluminum content was lower due to the more severe reaction conditions.

Optical examination of cross-sections of the reaction interface suggests that the removal of aluminum from both  $\text{NiAl}_2$  and  $\text{Ni}_2\text{Al}_3$  is an "advancing interface" type process and not a reaction proceeding via intermediate compounds or the progressive removal of aluminum over the whole particle. Electron probe microanalysis shows the absence of gradients of aluminum concentration at the reaction interface and equivalent aluminum concentrations in the reacted zone of partly extracted alloy to those in the final catalyst. The data of Sassoulas and Trambouze (2), who found that  $\text{Ni}_2\text{Al}_3$  and nickel were the only crystalline phases detectable in partially extracted  $\text{Ni}_2\text{Al}_3$ , is consistent with such a process.

Sassoulas and Trambouze (2) also report that pure  $\text{NiAl}_2$  reacts more readily with aqueous sodium hydroxide than pure  $\text{Ni}_2\text{Al}_3$ . This is found to be equally true of these phases in the present multicomponent alloys. Thus, when reaction was carried out in an excess of concentrated alkali in the normal way, markedly preferential reaction of  $\text{NiAl}_2$  was observed (Fig. 5). Literature data involving partly extracted catalyst must therefore be interpreted with care; for example, the hydrogen evolved may not be a good measure of the fraction of the nickel that has been activated.

The nonselective reaction, reported by Mason (5) and thought to signify a difference in behavior between the pure phases and the multiphase alloy, has been shown to result from a different method of catalyst preparation in which the amount of sodium hydroxide does not satisfy the stoichiometric requirements of Eq. (1). Dirksen and Linden (9) suggested two possible contributory reactions in addition to Eq. (1):



Equation (1) appears to offer an adequate description of the standard activation process. The hydrolysis of sodium aluminate [Eq. (3)] during subsequent water washing may well yield much of the

$\beta$   $\text{Al}_2\text{O}_3 \cdot 3\text{H}_2\text{O}$  known (10) to exist in the final catalyst. The IGT activation process may well involve a combination of (1) and (3), the necessary alkali ions being continually regenerated by the hydrolysis reaction to yield the high alumina content of these catalysts reported by Dirksen and Linden (9) and confirmed in the present study. The IGT and the normal activation processes lead to similar products with small nickel crystallites (5), comparable porosity (7) and catalytic activity (15). Apparently, the low alkali concentration in the former method is reflected only in the large amounts of hydrated alumina present. The equivalent rates of reaction of  $\text{NiAl}_2$  and  $\text{Ni}_2\text{Al}_3$  in the IGT activation is presumably caused by a change in rate-determining step between the two extraction methods.

#### ACKNOWLEDGMENTS

The authors are grateful to the Davison Chemical Co. Ltd., for fellowship funds, to Dr. F. G. Clapette and N. E. Miller for catalyst samples and helpful discussions, to Professor G. R. Purdy and H. W. Walker, for guidance in the interpretation of results and the operation of the electron probe microanalyzer of the Metallurgy and Material Science Department, and to the National Research Council for providing the electron probe.

#### REFERENCES

1. LAEGER, E., AND MOHRITZ, F. L., *Advan. Catalysis* 5, 417 (1953).
2. SASSOULAS, R., AND TRAMBOUZE, Y., *Bull. Soc. Chim. France* 5, 985 (1964).
3. ALEXANDER, W. O., AND VAUGHAN, W. B., *J. Inst. Metals* 61, 247 (1937).
4. LITTMAN, H., AND BLIZZ, H., *Ind. Eng. Chem.* 51, 662 (1959).
5. MASON, D. McA., in Ref. (9).
6. KANIKV, T., FASMAN, A. B., ISABERKOV, A., AND CHERNOUSOVA, K. T., *Elektrokhimiya* 1, 568 (1965).
7. FRIEL, J., PIETSKH, W. J. M., AND ANDERSON, R. B., *J. Catalysis* 14, 247 (1969).
8. ROSTOKER, W., AND DVORAK, J. R., "Interpretation of Metallographic Structures," Chap. 5. Academic Press, New York, 1965.
9. DIRKSEN, H. A., AND LINDEN, H. R., *Inst. Ges. Technol. Res. Bull.* 31, (1963), 137.
10. KOKES, R. J., AND EMMETT, P. H., *J. Am. Chem. Soc.* 81, 5032 (1959).



11. FRENZ, J., ROBERTSON, S. D., AND ANDERSON, R. B., *J. Catalysis*, submitted for publication.
12. CASTAING, R., in "Third International Sym-

posium on X-Ray Optics and X-Ray Microanalysis" (H. H. Pattee, V. E. Coslett, and A. Jorgensen, eds.), p. 203. Academic Press, New York, 1963.

## Effect of Ni-Al Precursor Alloy on the Catalytic Activity for a Raney-Ni Cathode

Shin-ichi Tanaka,<sup>a,b,\*</sup> Norimitsu Hirose,<sup>c</sup> Toshiyuki Tanaka,<sup>c</sup> and Yukio H. Ogata<sup>b,\*</sup>

<sup>a</sup>Tokyo Metropolitan Industrial Technology Research Institute, Kizu-ku, Tokyo 115-8586, Japan

<sup>b</sup>Institute of Advanced Energy, Kyoto University, Uji, Kyoto 611-0011, Japan

<sup>c</sup>Tokyo Metropolitan Eastern District Small and Medium-Sized Business Promotion Center, Katashika-ku, Tokyo 125-0062, Japan

Raney-Ni cathodes were prepared by leaching aluminum from Ni-Al precursor alloys (NiAl<sub>3</sub>, Ni<sub>2</sub>Al<sub>3</sub>, NiAl, and Ni<sub>3</sub>Al). The catalytic activity for the hydrogen evolution reaction was investigated in 1 M NaOH at 303 K. The hydrogen overpotentials of Raney-Ni electrodes obtained from NiAl<sub>3</sub> and Ni<sub>2</sub>Al<sub>3</sub> were lower than those from nickel rich alloys (NiAl and Ni<sub>3</sub>Al). Especially, NiAl<sub>3</sub> yielded the most active Raney-Ni cathode. This is because the fast aluminum leaching from NiAl<sub>3</sub> phase gives large surface area of the electrode, the formation of small micropores, and the appearance of the Ni phase.

© 2000 The Electrochemical Society. S0013-4651(99)09-012-6. All rights reserved.

Manuscript submitted September 3, 1999; revised manuscript received January 28, 2000.

H<sub>2</sub> is one of the most promising energy carriers and storage media. Although H production by water electrolysis is a well-established technology, its cost is still too high in contrast to the H obtained from hydrocarbon sources. There is no doubt that the electricity expense is the largest factor for electrolytic production of H, and varies with the cell potential. Great efforts have been made toward reduction through developing adequate hardware designs and through surveying optimum operation conditions for electrolysis. Of these, development of low H overvoltage cathode is one of the key factors. Many attempts have been made to develop efficient and durable electrode materials for H evolution reactions in alkaline solution. The Raney-Ni is one of the best electrodes, since it is inexpensive, highly active, and without a noble metal.<sup>1-13</sup> The Raney-Ni catalysts are obtained by leaching Al out of precursor Ni-Al alloys in concentrated NaOH solution. This leaching procedure provides a high surface area, resulting in the reduction of H overvoltage. The precursor alloy is prepared practically by melting Ni and Al, where the composition is around fifty-fifty in weight, and usually contains some types of intermetallic compounds: NiAl<sub>3</sub>, Ni<sub>2</sub>Al<sub>3</sub>, NiAl, and Ni<sub>3</sub>Al.<sup>14</sup> The phases behave differently in the leaching process and affect the morphology, composition, and catalytic activity. However, the role of each compound in the catalytic activity of the Raney-Ni cathode has been not clarified. We should use the precursor alloy consisting of one phase to understand the Raney-Ni electrode deeply.

In this study, the Raney-Ni electrodes were prepared from various precursor Ni-Al alloys. We investigated the electrochemical activities of these electrodes and the effect of precursor alloy. These Raney-Ni electrodes were also characterized by X-ray diffraction (XRD) analysis and N<sub>2</sub> gas adsorption method.

### Experimental

**Preparation of electrode.**—Ni-Al precursor alloys (NiAl<sub>3</sub>, Ni<sub>2</sub>Al<sub>3</sub>, NiAl, and Ni<sub>3</sub>Al) were prepared from Ni (99.95% pure) and Al (99.99% pure) shots. The shots were weighted according to the stoichiometry of each alloy and melted in an alumina crucible using an induction furnace. Each ingot was annealed to homogenize at 973 K for 4 h in a vacuum furnace, the base pressure of which was under  $5 \times 10^{-3}$  Torr. The formation of Ni-Al intermetallic compounds was confirmed by XRD, as shown in Fig. 1. These intermetallic compounds were cut with a silicon base saw into an appropriate size. The electrical contact was made by joining a copper wire with silver epoxy resin. The electrode was polished with emery paper using deionized water as lubricant. The leaching of Al was accomplished by dipping in 6 M NaOH at 343 K for 1 h. We hereafter denote Raney-Ni cathodes thus prepared from NiAl<sub>3</sub>, Ni<sub>2</sub>Al<sub>3</sub>, NiAl, and Ni<sub>3</sub>Al alloys as R<sub>13</sub>, R<sub>23</sub>, R<sub>11</sub>, and R<sub>31</sub>, respectively.

\* Electrochemical Society Active Member.

**Electrochemical measurements and surface analysis.**—Polarization measurements of the cathodes were conducted galvanostatically in 1 M NaOH at 303 K. The electrode was positioned in a Pyrex glass cell of about 0.5 dm<sup>3</sup>. A platinum plate was used as the counter electrode. The electrolyte was pre-electrolyzed with a couple of platinum electrodes in a polytetrafluoroethylene (PTFE) cell at 100 A/dm<sup>2</sup> for 24 h to remove trace impurities and then transferred to the measurement cell. Such a procedure was very important to avoid problems caused by contamination and to obtain reproducible results. The cathode potential was measured using a Luggin-Haber probe in connection with a reversible hydrogen electrode (RHE) placed in the same solution. The solution ohmic drop between the working electrode and the probe was corrected using current interruption technique. Therefore, measured potential corresponds to H overpotential.

Impedance measurements were performed for evaluating the effective surface area of electrodes. The measurements were carried out at -0.1 V vs. RHE. The frequency was varied in the range from 20 kHz to 10 mHz, and the ac amplitude was kept constant at 10 mV in rms.

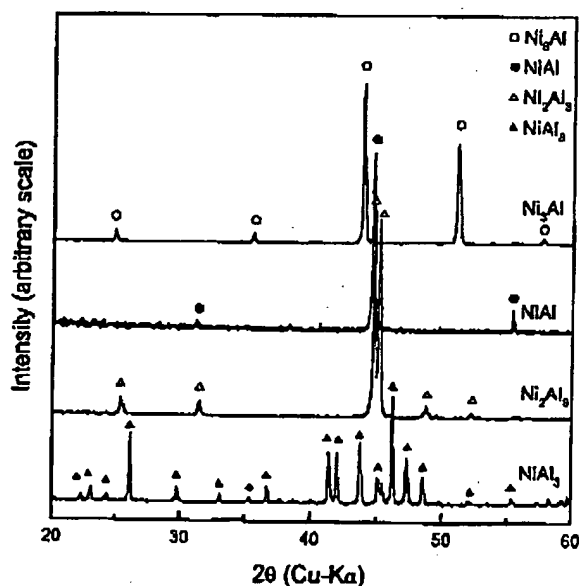


Figure 1. XRD patterns of Ni-Al precursor alloys before leaching Al.

The crystalline structure of the electrode was examined by XRD. The pore distribution was also measured by  $N_2$  gas adsorption.

### Results and Discussion

The electrochemical activity of the H evolution reaction was evaluated by measuring current density-potential ( $i$ - $E$ ) curves in 1 M NaOH at 303 K. The results are shown in Fig. 2. The corresponding kinetic parameters are summarized in Table I. The H overpotential of Raney-Ni cathodes prepared from  $NiAl_3$  and  $Ni_2Al_3$  was lower than those from Ni rich precursor alloys ( $NiAl$  and  $Ni_3Al$ ). The H overpotentials at 25 A/dm<sup>2</sup> ( $\eta_{25}$ ) of  $R_{13}$  and  $R_{23}$  were -0.19 and -0.32 V, respectively, while  $R_{11}$  and  $R_{31}$  indicated  $\eta_{25} = -0.48$  and -0.51 V, respectively.  $E - \log i$  relations for  $R_{13}$  and  $R_{23}$  deviated from linearity, and hence, the kinetic parameters could not be estimated from the polarization curves. Raney-Ni electrodes usually have micropores on the surfaces. The nonlinearity of the slope is caused by concentration polarization in the very narrow micropores or blocking of the electrode surface by H bubbles in these pores.<sup>13</sup> The distribution of micropore size for  $R_{13}$  and  $R_{23}$  was measured by  $N_2$  adsorption. These results are shown in Fig. 3. The radius of micropores in  $R_{13}$  mainly distributes below 30 Å. On the other hand, micropores of  $R_{23}$  have sizes smaller than 100 Å. This difference in size causes the result that the Tafel slope of  $R_{13}$  is larger than that of  $R_{23}$  (Fig. 2), although the reason is unknown so far. In contrast, cathodes prepared from Ni rich alloys,  $R_{11}$  and  $R_{31}$ , satisfied linearity in the Tafel plots, and the slope was about 0.12 V/dec. The charge transfer coefficient,  $\alpha_c$ , corresponds to ca. 0.5. It is suggested that the H evolution reaction proceeds on  $R_{11}$  and  $R_{31}$  through the same mechanism as on a Ni electrode. These results indicate that an active Raney-Ni cathode is obtained only from Al rich alloys  $NiAl_3$  and  $Ni_2Al_3$ .

The Raney-Ni cathode indicates the low Tafel slope in the industrial condition. For example, the Tafel slope for the Raney-Ni cathode, which was prepared by electrodeposition, was about 0.045 V/decade in 35 wt % NaOH at 363 K.<sup>3</sup> Chen *et al.*<sup>8</sup> reported a marked increase in activity at higher temperature: the Tafel slope of the Raney-Ni cathode was 0.09 and 0.04 V/decade in 1 M NaOH at 298 and 353 K, respectively. Pshenichnikov<sup>6</sup> also reported that Raney-Ni cathode indicated two Tafel slopes with 0.04 V/decade at the low current density region and 0.12 V/decade at the high current density region. In this study,  $R_{11}$  and  $R_{23}$  were indicated by two Tafel

Table I. Kinetic parameters of  $H_2$  evolution reactions on Ni and Raney-Ni electrodes prepared from various Ni-Al precursor alloys in 1 M NaOH at 303 K:  $i_0$ , exchange current density;  $b$ , Tafel slope;  $\alpha_c$ , charge transfer coefficient;  $\eta_{25}$ , H overpotential at 25 A/dm<sup>2</sup>.

Specimen	$i_0$ (A/dm <sup>2</sup> )	$b$ (V/decade)	$\alpha_c$ (-)	$\eta_{25}$ (V)
Ni	$1.09 \times 10^{-3}$	0.120	0.50	0.522
$R_{13}$	—	—	—	0.186
$R_{23}$	—	—	—	0.316
$R_{11}$	$2.55 \times 10^{-3}$	0.121	0.50	0.475
$R_{31}$	$9.19 \times 10^{-4}$	0.115	0.52	0.509

regions, although  $E - \log i$  relations deviated from linearity at high current density region. The transition point from low to high Tafel slope would be shifted to the direction of high current density when the solution temperature was high such as an industrial condition. Therefore, the H overvoltage at high current density probably indicated lower value at high temperature NaOH solution.

An active Raney-Ni is usually prepared from the Ni-Al precursor alloy which has a mass fraction of 50 wt % Ni and the rest consists of Al. The four types of intermetallic compounds generally exist in the Ni-Al alloy system; however the composition of the Ni-Al precursor alloy is not clarified. The dissolution rate of Al from these precursor alloys is a very important factor because an active Raney-Ni is obtained by leaching Al out of the precursor alloy in concentrated NaOH solution. The difference of the catalytic activity in Raney-Ni cathodes probably depends on the dissolution rate of Al from Ni-Al intermetallic compounds in concentrated NaOH solution. In order to investigate the leaching rate from each Ni-Al precursor alloy, the weight loss due to leaching Al was measured in 1 M NaOH at 303 K. These results are shown in Fig. 4. This leaching condition was chosen to prevent the disintegration of Ni-Al intermetallic compounds during leaching. The weight loss was observed only for Al rich alloys ( $NiAl_3$  and  $Ni_2Al_3$ ) in this leaching condition. Especially, Al was leached much more readily from  $NiAl_3$  than from  $Ni_2Al_3$ . On the other hand, NaOH solution could not leach out an

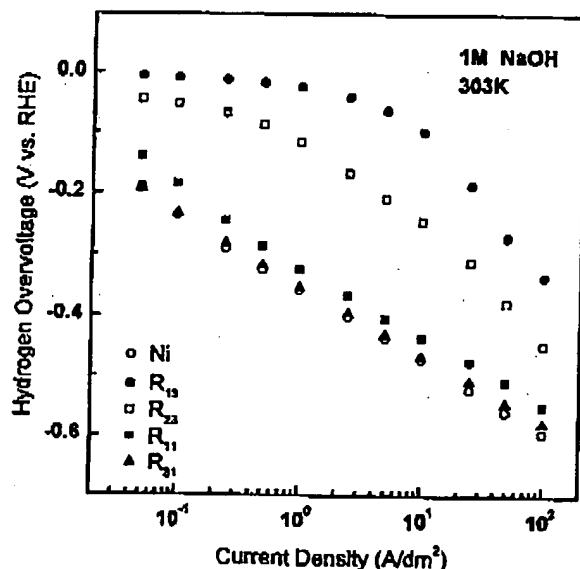


Figure 2. Cathodic polarization curves for  $H_2$  evolution reaction in 1 M NaOH at 303 K on a Ni and an electrode obtained from various Ni-Al precursor alloys after leaching.

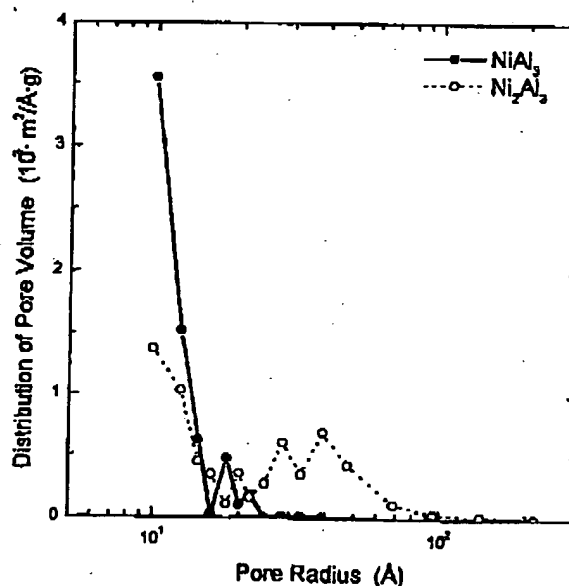


Figure 3. Micropore distribution in  $NiAl_3$  and  $Ni_2Al_3$  after leaching Al in 6 M NaOH at 343 K for 1 h.

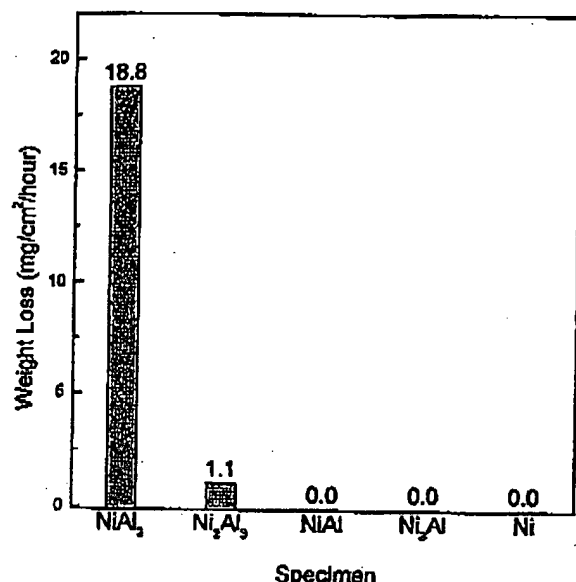


Figure 4. Weight loss of Ni-Al precursor alloys during leaching in 1 M NaOH at 303 K for 1 h.

appreciable amount of Al from Ni rich alloys (NiAl and Ni<sub>2</sub>Al). These results show that an active Raney-Ni cathode can be produced only by leaching of NiAl<sub>3</sub> or Ni<sub>2</sub>Al<sub>3</sub>. According to Bakker *et al.*,<sup>16</sup> NiAl<sub>3</sub> was leached more rapidly than Ni<sub>2</sub>Al<sub>3</sub> phase. In addition, the leaching of NiAl<sub>3</sub> proceeded even if the temperature of NaOH was low. In this study, rapid dissolution of Al from NiAl<sub>3</sub> is in good agreement with their results. Although they also reported that the leaching of Ni<sub>2</sub>Al<sub>3</sub> phase did not proceed below 343 K, we observed the dissolution of Al from Ni<sub>2</sub>Al<sub>3</sub> at 303 K by the weight loss and the H evolution during leaching.

The catalytic activity for H evolution reaction is affected by the effective surface area of the electrode. To estimate the relative surface area of electrodes, the double layer capacitance was derived by ac impedance measurements. The relative surface area was deduced from the double layer capacitance. The capacitance was calculated with a complex nonlinear least-squares program developed by Macdonald,<sup>17</sup> because the flattened semicircles were observed on the complex plan plots. The equivalent circuit model consists of the solution resistance in series with a parallel connection of the double layer capacitance and the faradaic impedance which is usually represented as a simple charge transfer resistance. In this model, the double layer capacitance is submitted by a constant phase element. The results are shown in Table II. R<sub>13</sub> and R<sub>23</sub> electrodes had 10<sup>4</sup> times larger surface area than a Ni electrode. Since Al from Ni<sub>2</sub>Al<sub>3</sub> phase dissolves more slowly than from NiAl<sub>3</sub> under the same leaching condition, the R<sub>13</sub> electrode obtained from NiAl<sub>3</sub> has a

Table II. Relative surface area of Raney-Ni electrodes determined by ac impedance in 1 M NaOH at -0.1 V vs. RHE. C<sub>dl</sub> is double layer capacitance.

Specimen	C <sub>dl</sub> (μF/cm <sup>2</sup> )	Relative surface area ( )
Ni	52	1
R <sub>13</sub>	836 × 10 <sup>3</sup>	12667
R <sub>23</sub>	617 × 10 <sup>3</sup>	9348
R <sub>11</sub>	55	1.1
R <sub>31</sub>	58	1.1

higher surface area than the R<sub>23</sub>. On the contrary, the surface areas of cathodes from R<sub>11</sub> and R<sub>31</sub> were nearly equal to Ni, because Al was hardly leached. In consequence, the R<sub>11</sub> and R<sub>31</sub> display lower catalytic activity than those from Al rich alloys. Especially, R<sub>13</sub> provides the highest activity. However, the catalytic activity of the Raney-Ni cathode could not be explained only with the surface area, because the surface composition on Raney-Ni after leaching affects the catalytic activity. The leaching process is not complete, generally, and a small amount of less noble metal remains in Raney-Ni.<sup>18,19</sup> The amount of residual Al in the electrode obtained from Ni<sub>2</sub>Al<sub>3</sub> is probably more than that from NiAl<sub>3</sub>, because the dissolution rate of aluminum from NiAl<sub>3</sub> phase is more rapid than that from Ni<sub>2</sub>Al<sub>3</sub>. The residual Al in R<sub>23</sub> affects the open circuit potential, shifting to slightly more negative than the H<sub>2</sub>O/H<sub>2</sub> thermodynamic equilibrium potential. Indeed, the static potentials in 1 M NaOH at 303 K for R<sub>13</sub> and R<sub>23</sub> were -4 and -43 mV, respectively. In addition, the R<sub>13</sub> electrode shows higher catalytic activity than the R<sub>23</sub> as already described. The results indicated that an increase of the residual Al content in Raney-Ni leads to the decrease of the catalytic activity.

Figure 5 shows XRD patterns for Ni-Al electrodes after leaching in 6 M NaOH at 343 K for 1 h. Since Al hardly dissolves from Ni rich alloys in the NaOH solution, XRD peaks of NiAl and Ni<sub>2</sub>Al did not undergo significant changes. In the case of R<sub>23</sub>, the peaks from the Ni<sub>2</sub>Al<sub>3</sub> phase were detected, but they were broadened. Bakker *et al.*<sup>16</sup> reported that Ni<sub>2</sub>Al<sub>3</sub> was converted to a mixture of Ni<sub>2</sub>Al<sub>3</sub> and Ni during the leaching and the leaching of Ni<sub>2</sub>Al<sub>3</sub> proceeded according to the selective dissolution mechanism. Although the selective dissolution reaction produces the composite of Ni<sub>2</sub>Al<sub>3</sub> and Ni during leaching, the complete leaching yields only Ni phase. In this study, the Ni peak is not observed on the XRD chart after leaching. The dissolution rate of Al from Ni<sub>2</sub>Al<sub>3</sub> is very slow (Fig. 4), so that the production of Ni phase is not observed in this leaching condition. The presence of Ni<sub>2</sub>Al<sub>3</sub> phase in the Raney-Ni cathode leads to a decrease of the catalytic activity for H<sub>2</sub> evolution;<sup>18</sup> besides, it is reported that the phase of Ni appeared on the XRD chart when Ni<sub>2</sub>Al<sub>3</sub> was leached until no more H<sub>2</sub> gas evolved.<sup>18,19</sup> If the leaching condition were more severe (e.g., at high temperature, or for a long time), even the Ni<sub>2</sub>Al<sub>3</sub> phase would be dissolved and transformed into the Ni phase. Therefore, the leaching condition would play an important role in the catalytic activity.

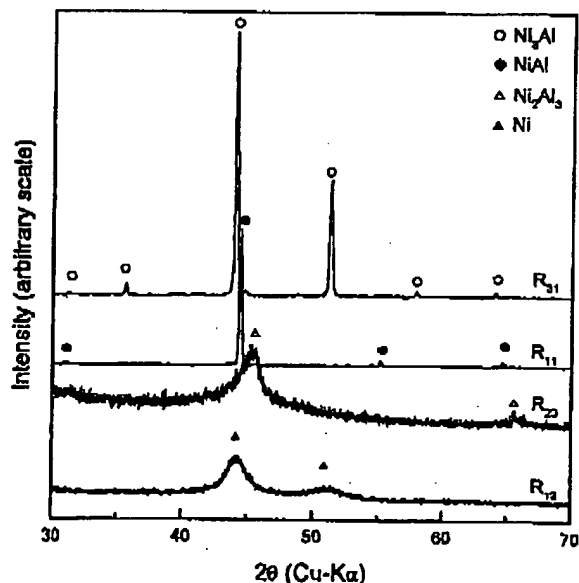


Figure 5. XRD patterns of Ni-Al precursor alloys after leaching Al in 6 M NaOH for 1 h at 343 K.

On the contrary, the XRD pattern of  $R_{13}$  exhibited that there was no peak from the Ni-Al alloy but broad peaks from Ni appeared instead. The broadening of XRD peaks may be attributed to the appearance of an amorphous structure,<sup>8,11,12</sup> a small crystallite size, and lattice defects or internal stress, although we cannot determine which cause is applicable to the present experiment. Choudhary *et al.*<sup>20,21</sup> suggested that the leaching proceeded in various stages involving phase transformation:  $NiAl_3 \rightarrow Ni_2Al_3 \rightarrow NiAl \rightarrow Ni$ . Choquette *et al.*<sup>1</sup> also reported that  $NiAl_3$  was transformed into  $Ni_2Al_3$  during leaching. However, the transformation of  $NiAl_3$  into  $Ni_2Al_3$  is not observed in this study. If  $NiAl_3$  were converted into  $Ni_2Al_3$  during leaching, the peak of  $Ni_2Al_3$  should be observed on the XRD of  $R_{13}$  because the dissolution of Al from  $Ni_2Al_3$  is slower than that from  $NiAl_3$ . In addition,  $NiAl$  phase does not dissolve in NaOH solution, so that the  $NiAl$  peak should be also detected on the XRD of  $R_{13}$  and  $R_{23}$ . However, the XRD pattern of  $NiAl_3$  after leaching shows only the Ni phase in this study. This result implies that  $NiAl_3$  and  $Ni_2Al_3$  phases are directly transformed into Ni during the leaching of Al.

The Ni-Al precursor alloy commonly contains 50 wt % Ni and 50 wt % Al. The precursor alloy has low strength, substantially no impact strength, and cannot be fabricated by conventional technique. The product is, therefore, provided as a powder. An active Raney-Ni electrode is prepared by electrochemical codeposition of the suspended powder from Ni plating bath.<sup>1-5</sup> If the  $NiAl_3$  powder would be substituted for the conventional powder, 50 wt % Ni, the electrocatalytic activity of the Raney-Ni cathode could increase. However, the catalytic activity of the Raney-Ni electrode prepared from electrochemical codeposition is affected by electroplating conditions. Further detailed investigation is necessary to adopt the  $NiAl_3$  powder for electroplating.

#### Conclusion

The Raney-Ni cathodes were prepared by leaching Al from various Ni-Al precursor alloys ( $NiAl_3$ ,  $Ni_2Al_3$ ,  $NiAl$ , and  $Ni_3Al$ ). An active Raney-Ni electrode was obtained only from Al rich alloys ( $NiAl_3$  and  $Ni_2Al_3$ ) because the dissolution of Al from these alloys proceeded in NaOH solution. Especially, the most active Raney-Ni

cathode was yielded from  $NiAl_3$  due to the rapid Al leaching. On the other hand,  $Ni_2Al_3$  phase is present in  $R_{23}$ , which decreases the catalytic activity. Because the large surface of the electrode, the formation of the micropores, and the appearance of Ni phase after leaching Al,  $R_{13}$  indicated low H overpotential.

#### Acknowledgments

The authors thank Dr. K. Sato of Tokyo Metropolitan Industrial Technology Research Institute for the preparation of Ni-Al precursor alloys. The authors also thank Dr. T. Tsuboi of Kyoto University for useful discussion.

Tokyo Metropolitan Industrial Technology Research Institute assisted in meeting the publication costs of this article.

#### References

1. Y. Choquette, L. Brossard, and H. Meaard, *J. Appl. Electrochem.*, **20**, 855 (1990).
2. E. Eadoh, H. Ootsuma, T. Morimoto, and Y. Oda, *Int. J. Hydrogen Energy*, **12**, 473 (1987).
3. E. Eadoh, H. Ootsuma, T. Morimoto, and Y. Oda, *Nippon Kagaku Kaishi*, no. 6, 858 (1988).
4. E. Eadoh, H. Ootsuma, and T. Morimoto, *Int. J. Hydrogen Energy*, **13**, 207 (1988).
5. J. K. Depo, M. Okido, G. A. Capuano, and R. Harris, *Can. Metall. Q.*, **33**, 369 (1994).
6. A. G. Pshenichnikov, *Int. J. Hydrogen Energy*, **7**, 51 (1982).
7. D. B. Hall, *J. Appl. Electrochem.*, **14**, 107 (1984).
8. L. Chen and A. Lasia, *J. Electrochem. Soc.*, **140**, 2464 (1993).
9. L. Chen and A. Lasia, *J. Electrochem. Soc.*, **139**, 1058 (1992).
10. K. Lahrberg and P. Kolli, *Electrochim. Acta*, **29**, 1357 (1984).
11. L. Chen and A. Lasia, *J. Electrochem. Soc.*, **138**, 3321 (1991).
12. L. Chen and A. Lasia, *J. Electrochem. Soc.*, **139**, 3214 (1992).
13. A. Rami and A. Lasia, *J. Appl. Electrochem.*, **22**, 376 (1992).
14. J. C. Klein and D. M. Hercules, *Anal. Chem.*, **53**, 754 (1981).
15. J. Freil, W. J. Pleton, and R. B. Anderson, *J. Catal.*, **16**, 281 (1970).
16. M. L. Bakker, D. J. Young, and M. S. Wainwright, *J. Mater. Sci.*, **23**, 3921 (1988).
17. J. R. Macdonald, *Impedance Spectroscopy*, John Wiley & Sons, New York (1987).
18. S. Tanaka, N. Hirose, and T. Tanaki, *Denki Kagaku oyobi Kogyo Bunsui Kagaku*, **65**, 637 (1997).
19. S. Tanaka, N. Hirose, and T. Tanaki, *Denki Kagaku oyobi Kogyo Bunsui Kagaku*, **65**, 1044 (1997).
20. V. R. Choudhary and S. K. Chaudhari, *J. Chem. Tech. Biotechnol.*, **33A**, 339 (1983).
21. V. R. Choudhary, S. K. Chaudhari, and A. N. Gokarn, *Ind. Eng. Chem. Res.*, **28**, 33 (1989).

## Catalytic Properties of Ni<sub>3</sub>Al Intermetallics for Methanol Decomposition\*

Ya Xu<sup>1</sup>, Satoshi Kameoka<sup>2</sup>, Kyosuke Kishida<sup>1</sup>, Masahiko Demura<sup>1</sup>,  
An-pang Tsai<sup>1,2</sup> and Toshiyuki Hirano<sup>1</sup>

<sup>1</sup>Materials Engineering Laboratory, National Institute for Materials Science, Tsukuba 305-0047, Japan

<sup>2</sup>Institute of Multidisciplinary Research for Advanced Materials, Tohoku University, Sendai 980-8577, Japan

Ni<sub>3</sub>Al is known as promising high-temperature structural materials because of its excellent high temperature strength and corrosion/oxidation resistance. Recently, we found that Ni<sub>3</sub>Al shows high activity for methanol decomposition ( $\text{CH}_3\text{OH} \rightarrow 2\text{H}_2 + \text{CO}$ ), and little effect for steam reforming of methanol ( $\text{CH}_3\text{OH} + \text{H}_2\text{O} \rightarrow 3\text{H}_2 + \text{CO}_2$ ) in the case of feeding methanol and water. In the present study, we examined the catalytic activity of Ni<sub>3</sub>Al powders by feeding pure methanol at a reaction temperature range from 523 to 633 K. It was found that Ni<sub>3</sub>Al shows not only a high activity for the methanol decomposition but also suppresses the methanation. The catalytic properties of Ni<sub>3</sub>Al were compared to that in the case of feeding both methanol and water.

(Received April 27, 2004; Accepted September 27, 2004)

**Keywords:** nickel aluminides, Ni<sub>3</sub>Al, intermetallics, catalysis, methanol decomposition

### 1. Introduction

Methanol decomposition to hydrogen and carbon monoxide is an important reaction for methanol-fuelled vehicles and utilization of waste heat from industries. It is known that nickel catalysts are active for methanol decomposition. However, they have a drawback of the formation of methane due to the chemical reaction between product gases, hydrogen and carbon monoxide.<sup>1-3)</sup> It is, therefore, necessary to develop better catalysts without causing methanation. Some intermetallic compounds are known to have good catalytic selectivity and activity. For example, Ni<sub>3</sub>Sn increases the selectivity for hydrogen production,<sup>3)</sup> and PtGe and CoGe do for hydrogenation.<sup>4,5)</sup> In Ni-Al system there are four stable intermetallic compounds, NiAl<sub>3</sub>, Ni<sub>2</sub>Al<sub>3</sub>, NiAl and Ni<sub>3</sub>Al. Among them a mixture of NiAl<sub>3</sub> and Ni<sub>2</sub>Al<sub>3</sub> (Ni-50 mass% Al) is used as a precursor alloy for Raney nickel catalysts: the Raney nickel catalysts are produced from the precursor alloy by leaching aluminum in a concentrated NaOH solution. For NiAl and Ni<sub>3</sub>Al, very limited studies have been carried out on the catalytic properties. Probably it has been thought difficult to effectively leach aluminum from them because of their low aluminum concentration,<sup>6)</sup> and thus high catalytic activity has not been expected, particularly for Ni<sub>3</sub>Al. Until now, Ni<sub>3</sub>Al is known as promising high-temperature structural materials because of its excellent high temperature strength and corrosion/oxidation resistance and thus many studies have been focused on the mechanical properties and the microstructures.<sup>7-9)</sup> Recently, we studied the catalytic properties of Ni<sub>3</sub>Al for hydrogen production from the mixture of methanol and water. It was found that Ni<sub>3</sub>Al shows high activity and selectivity for methanol decomposition and little effect of water on the reaction.<sup>10)</sup> In the present study, we studied the catalytic activity of Ni<sub>3</sub>Al for hydrogen production from pure methanol in order to examine the effect of water.

### 2. Experimental

The sample preparation is the same as the previous study.<sup>10)</sup> Ni<sub>3</sub>Al (Ni-12.7 mass% Al) alloy ingot was prepared by conventional induction heating and homogenized at 1573 K for 36 ks in high vacuum. Then the ingot was scrapped with a planer machine, crushed to powder less than 150  $\mu\text{m}$  in size by mechanical milling. The powder was dipped in a stirring 20 mass% NaOH aqueous solution at 340 K for 18 ks in order to leach aluminum. After leaching the NaOH solution was subjected to inductively coupled plasma (ICP) analysis in order to measure the amount of leached aluminum. The surface area of the powder was determined by BET (Brunauer-Emmett-Teller) surface area analysis. The crystal structure before and after leaching was analyzed by X-ray diffraction (XRD) using a CuK $\alpha$  source (Rigaku, RINT2500). For comparison, a nickel catalyst was prepared by the same leaching treatment as the Ni<sub>3</sub>Al powder from commercial Ni-50 mass% Al alloy powder (Raney-Nickel, Mitsuwa Chemicals).

The catalytic experiments of methanol decomposition from methanol were carried out in a conventional fixed-bed flow reactor as described in the previous report.<sup>10,11)</sup> The Ni<sub>3</sub>Al powder of 0.2 g was set in a quartz tube with an internal diameter of 8 mm in the reactor. Prior to reaction, the powder was reduced at 513 K for 3.6 ks in a flowing hydrogen atmosphere. Then, the hydrogen flow was stopped and refilled with nitrogen to flush H<sub>2</sub>. Subsequently pure methanol was introduced to the quartz tube at a liquid hourly space velocity of 30 h<sup>-1</sup> (defined as the volume of methanol passed over the unit volume of catalyst per hour) using a plunger pump together with nitrogen carrier gas. Reaction temperature was increased stepwise from 513 to 633 K at intervals of 20 K. The outlet composition of gas products was analyzed after 1.5 ks at each temperature using gas chromatograph (Shimadzu, GC-14B equipped with thermal conductivity detectors (TCD)).

### 3. Results and Discussion

The amount of leached aluminum was estimated at

\*This Paper was Presented at the Spring Meeting of the Japan Institute of Metals, held in Tokyo, on March 30, 2004.

Table 1 Results of BET surface area measurements ( $\text{m}^2/\text{g}$ )

	Before leaching	After leaching
$\text{Ni}_3\text{Al}$	2.3	5.1
Ni catalyst	1.8	2.8

13.9 mass% of aluminum concentration in the precursor  $\text{Ni}_3\text{Al}$  by ICP analysis. No nickel was detected in the solution. In the case of the nickel catalyst, much larger amount of aluminum was leached in the same process as  $\text{Ni}_3\text{Al}$ . The amount of leached aluminum was estimated at 78.4 mass% of aluminum concentration in the precursor  $\text{Ni}_3\text{Al}$  alloy.

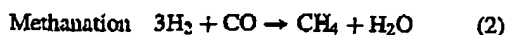
The results of the BET surface area measurement were summarized in Table 1. It is found that the surface area increases more than twice by leaching. The BET measurement showed that the surface pore radius is sharply distributed at approximately 2 nm after leaching, indicating that the observed increase in surface area is due to the formation of these fine pores. For the nickel catalyst used for comparison, the surface area after leaching,  $2.8 \text{ m}^2/\text{g}$ , is smaller than that of the  $\text{Ni}_3\text{Al}$  catalyst. This is ascribed to the fact that the nickel catalyst was dried in air. Probably the surface of the nickel catalyst was oxidized during the drying process, resulting in the reduction in surface area since they are very reactive in air. However, the characteristics of the nickel catalyst are not qualitatively damaged by this process, which will be described below.

Figure 1(a) shows the XRD results of the  $\text{Ni}_3\text{Al}$  powder before and after leaching. All the diffraction peaks observed are assigned as  $\text{Ni}_3\text{Al}$ . No significant difference is observed between before and after leaching. These results indicate that leaching of aluminum is limited to the very thin surface layer of the  $\text{Ni}_3\text{Al}$  powder, leaving the bulk as it was. On the other hand, in the case of the nickel catalyst as shown in Fig. 1(b), the diffraction peaks observed before alkali leaching are assigned as  $\text{NiAl}_3$  and  $\text{Ni}_2\text{Al}_3$ , and fcc nickel phase was formed on the surface as a result of alkali leaching.

Figure 2 shows the rates of  $\text{H}_2$ ,  $\text{CO}$ ,  $\text{CO}_2$  and  $\text{CH}_4$  productions as a function of the reaction temperature for the  $\text{Ni}_3\text{Al}$ , compared with nickel catalysts. In the  $\text{Ni}_3\text{Al}$  catalyst,  $\text{H}_2$  and  $\text{CO}$  are the main products in the whole temperature range and that their production rate increases with increasing temperature. The results mean that the methanol decomposition mainly occurs.



Above 573 K the amount of  $\text{CH}_4$  increases slightly for the  $\text{Ni}_3\text{Al}$  catalyst, indicating that the following methanation occurs at high temperatures in addition to the methanol decomposition:



However, the amount of methane produced is so small that the production rate of  $\text{H}_2$  is not virtually affected in the temperature range of this study. For comparison, the results of the  $\text{Ni}_3\text{Al}$  in the case of feeding both methanol and water are shown as dotted lines in Fig. 2. It is found that  $\text{Ni}_3\text{Al}$  shows similar catalytic characteristics in both cases. How-

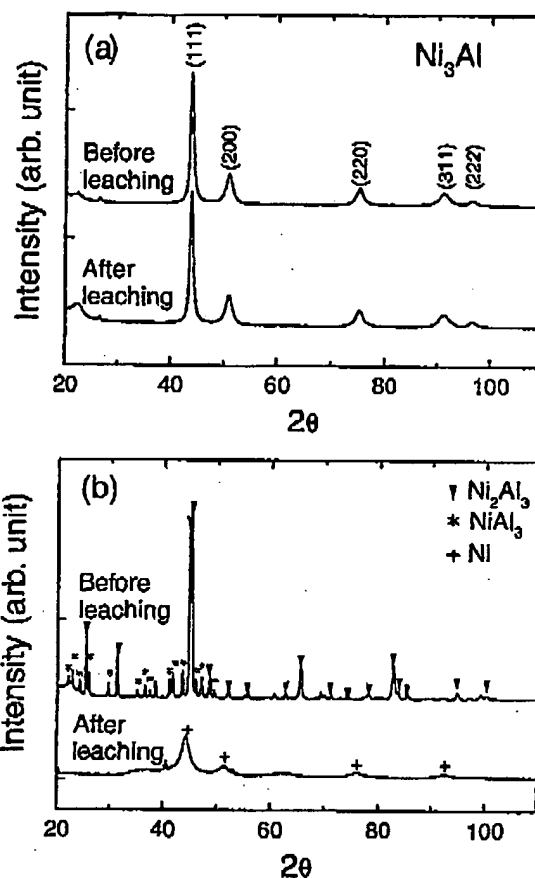


Fig. 1 XRD patterns of  $\text{Ni}_3\text{Al}$  (a) and Raney-nickel (b) powders before and after alkali-leaching.

ever, several differences are noticed between them. First, the rates of  $\text{H}_2$  and  $\text{CO}$  production in the case of feeding pure methanol are lower than those in the case of feeding both methanol and water. Second, even at temperatures above 573 K, the rate of  $\text{CO}_2$  production in the case of feeding pure methanol is much lower, and the rate of  $\text{CH}_4$  production is slightly higher than that in the case of feeding methanol and water, indicating that in the absence of water, the water gas shift reaction ( $\text{CO} + \text{H}_2\text{O} \rightarrow \text{CO}_2 + \text{H}_2$ ) is suppressed, while the methanation is slightly enhanced.

Comparing the results of the nickel catalyst, the nickel catalyst shows higher activity for methanol decomposition below 553 K than  $\text{Ni}_3\text{Al}$  catalyst, while the methanation and the water gas shift reaction are highly accelerated above 553 K, accompanying the significant increase of  $\text{CO}_2$  and  $\text{CH}_4$  production rates. These results are qualitatively in consistent with previous studies:<sup>10</sup> the nickel catalysts are active for methanol decomposition,<sup>12,13</sup> methanation,<sup>1,2,14</sup> and water gas shift reaction.<sup>15,16</sup> As a result of the reaction of methanol (2), the rate of  $\text{H}_2$  production saturates above 573 K. These results confirmed the advantage of the  $\text{Ni}_3\text{Al}$  catalysts over the nickel catalysts in terms of the high activity and selectivity for methanol decomposition at high temperatures above 553 K.

Considering that a part of aluminum was leached on the

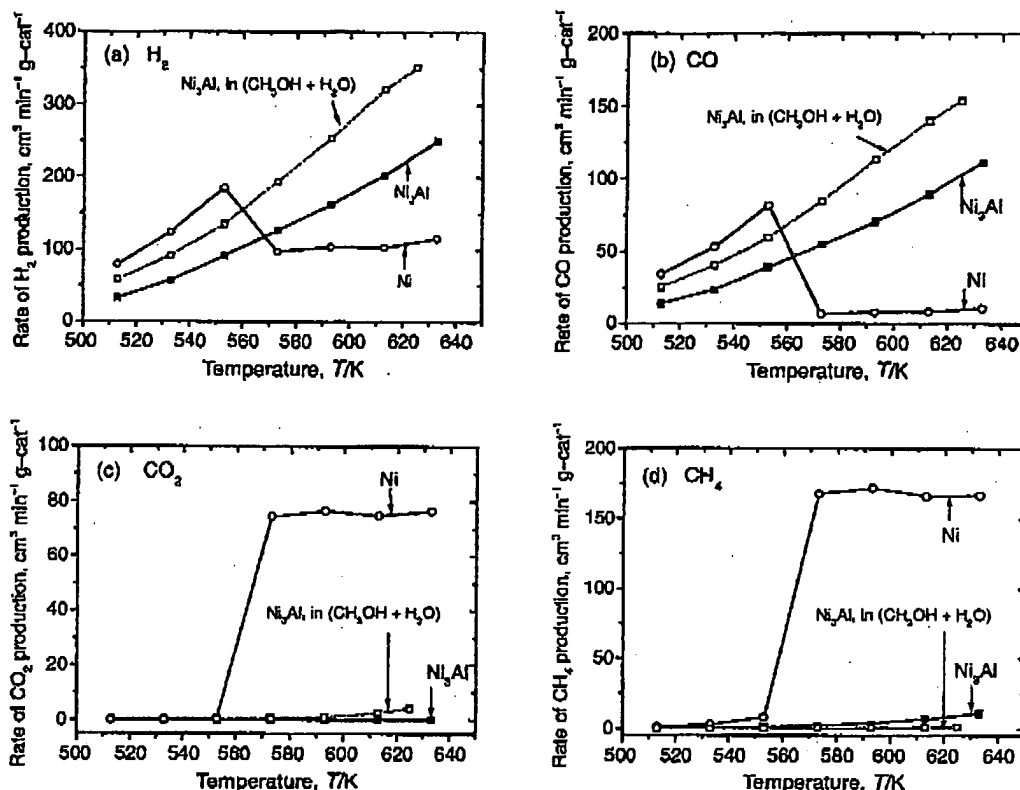


Fig. 2 The rates of (a) H<sub>2</sub>, (b) CO, (c) CO<sub>2</sub>, and (d) CH<sub>4</sub> production at various reaction temperatures from pure methanol for the alkali-leached Ni<sub>3</sub>Al and Raney-nickel catalysts (solid lines), and from the mixture of methanol and water for the alkali-leached Ni<sub>3</sub>Al (dotted lines).

surface of the Ni<sub>3</sub>Al powder, the outer surface of the Ni<sub>3</sub>Al must become nickel-enriched after leaching. It is, therefore, considered that the nickel-enriched surface, which may be a mixture of Ni<sub>3</sub>Al and nickel, increases the catalytic activity and the selectivity for methanol decomposition, by suppressing methanation. Detailed surface analysis is in progress.

#### 4. Conclusions

The catalytic activity of Ni<sub>3</sub>Al after alkali leaching was studied by feeding pure methanol in the temperature range of 513–633 K. The following results were obtained.

- (1) The alkali-leached Ni<sub>3</sub>Al catalyst in the case of feeding pure methanol shows similar catalytic characteristics to that in the case of feeding mixture of methanol and water, *i.e.* higher catalytic activity for the methanol decomposition than nickel catalyst above 573 K. The rate of hydrogen production increases rapidly with increasing reaction temperature.
- (2) The Ni<sub>3</sub>Al catalyst suppresses the formation of methane even in case of feeding pure methanol, *i.e.* it shows higher selectivity for methanol decomposition than nickel catalysts.

These results indicate that Ni<sub>3</sub>Al is highly promising as a catalyst for methanol decomposition.

#### REFERENCES

1. G. A. Mills and F. W. Steffgen: *Catalysis Rev.* **8** (1973) 159–210.
2. M. A. Vurmice: *Catal. Rev.-Sci. Eng.* **14** (1976) 153–191.
3. G. W. Huber, J. W. Shabaker and J. A. Dumesic: *Science* **300** (2003) 2075–2077.
4. T. Komatsu, S. Hyodo and T. Yashima: *J. Phys. Chem. B*, **101** (1997) 5565–5572.
5. T. Komatsu, M. Fukui and T. Yashima: *11th International Congress on Catalysis-40th Anniversary Studies in Surf. Sci. Catal.*, Vol. 101, Ed. by J. W. Hightower, W. N. Delgass, E. Iglesia and A. T. Bell, (Elsevier Science B. V, 1996) pp. 1095–1104.
6. S. Tanaka, N. Hirose, T. Tanaki and Y. H. Ogata: *J. Electrochemical Soc.* **147** (2000) 2242–2245.
7. D. P. Pope and S. S. Ezz: *Int. Mater. Rev.* **29** (1984) 136–167.
8. N. S. Stoloff: *Int. Mater. Rev.* **34** (1989) 153–183.
9. M. Yamaguchi and Y. Umakoshi: *Progress in Mater. Sci.* **34** (1990) 1–48.
10. Y. Xu, S. Kameoka, K. Kishida, M. Demura, A. P. Tsai and T. Hirano: *Intermetallics*, in press.
11. A. P. Tsai and M. Yoshimura: *Appl. Catal. A: General* **214** (2001) 237–241.
12. I. Yasumori, T. Nakamura and E. Miyazaki: *Bull. Chem. Soc. Jpn.* **40** (1967) 1372–1376.
13. B. Chen and J. L. Falconer: *J. Catal.* **144** (1993) 214–226.
14. J. Happel, I. Suzuki, P. Kokayeff and V. Fthenakis: *J. Catal.* **65** (1980) 59–77.
15. D. C. Grenoble, M. M. Estad and D. P. Ollis: *J. Catal.* **67** (1981) 90–102.
16. K. Mizuno, K. Yoshikawa and N. Wakejima: *Chem. Soc. Jpn. Chemistry Letters* (1986) 1969–1972.





## Catalytic properties of alkali-leached $\text{Ni}_3\text{Al}$ for hydrogen production from methanol

Ya Xu\*, Satoshi Kameoka, Kyosuke Kishida, Masahiko Demura,  
An-pang Tsai, Toshiyuki Hirano

*Light Materials Group, Materials Engineering Laboratory, National Institute for Materials Science, 1-2-1 Sezen, Tsukuba, Ibaraki 305-0047, Japan*

Received 20 April 2004; received in revised form 2 July 2004; accepted 9 July 2004  
Available online 11 September 2004

### Abstract

The catalytic properties of  $\text{Ni}_3\text{Al}$  intermetallics were studied for hydrogen production from methanol. It is found that the alkali-leached  $\text{Ni}_3\text{Al}$  powders show a high catalytic activity for the methanol decomposition ( $\text{CH}_3\text{OH} \rightarrow 2\text{H}_2 + \text{CO}$ ). The rate of hydrogen production increases rapidly with increasing reaction temperature. Furthermore, the  $\text{Ni}_3\text{Al}$  catalysts suppress the formation of methane and water gas shift reaction, i.e. they show higher selectivity for methanol decomposition than nickel catalysts. These results indicate that the  $\text{Ni}_3\text{Al}$  catalysts are highly promising as a catalyst for hydrogen production.

© 2004 Elsevier Ltd. All rights reserved.

**Keywords:** A. Nickel aluminides, based on  $\text{Ni}_3\text{Al}$ ; G. Catalysis

### 1. Introduction

Hydrogen is attracting much attention as a clean and efficient energy source. Many efforts have been made to develop efficient, low-cost catalysts for hydrogen production. Nickel catalysts are typical of them and have been widely used for hydrogen production. However, they have a drawback of the formation of methane due to the chemical reaction between product gases, hydrogen and carbon monoxide, which ends up in reducing the efficiency of hydrogen production [1–3]. It is, therefore, necessary to develop better catalysts without causing methanation.

Some intermetallic compounds are known to have good catalytic selectivity and activity. For example,  $\text{Ni}_3\text{Sn}$  increases the selectivity for hydrogen production [3], and  $\text{PtGe}$  and  $\text{CoGe}$  do for hydrogenation and dehydrogenation [4,5]. In  $\text{Ni-Al}$  system there are four stable intermetallic

compounds,  $\text{NiAl}_3$ ,  $\text{Ni}_2\text{Al}_3$ ,  $\text{NiAl}$  and  $\text{Ni}_3\text{Al}$ . Among them a mixture of  $\text{NiAl}_3$  and  $\text{Ni}_2\text{Al}_3$  (Ni–50 wt% Al) is used as a precursor alloy for Raney nickel catalysts: the Raney nickel catalysts are produced from the precursor alloy by leaching aluminum in a concentrated  $\text{NaOH}$  solution. For  $\text{NiAl}$  and  $\text{Ni}_3\text{Al}$ , very limited studies have been carried out on the catalytic properties. Probably, it has been thought difficult to effectively leach aluminum from them because of their low aluminum concentration [6], and thus high catalytic activity has not been expected, particularly for  $\text{Ni}_3\text{Al}$ . Until now,  $\text{Ni}_3\text{Al}$  is known as promising high-temperature structural materials because of its excellent high temperature strength and corrosion/oxidation resistance and thus many studies have been focused on the mechanical properties and the microstructures (for review, see Refs. [7–9]).

In the present study, we examined the catalytic activity of single-phase  $\text{Ni}_3\text{Al}$  powder for hydrogen production from methanol which is important in fuel cells and small-scale hydrogen plants [10]. We report here that  $\text{Ni}_3\text{Al}$  intermetallic compounds show not only a high activity for the methanol decomposition ( $\text{CH}_3\text{OH} \rightarrow 2\text{H}_2 + \text{CO}$ ), but also suppress the methanation.

\* Corresponding author. Tel.: +81-29-859-2573; fax: +81-29-859-2501.

E-mail address: [xu.ya@nims.go.jp](mailto:xu.ya@nims.go.jp) (Y. Xu).

## 2. Experimental

Ni<sub>3</sub>Al (Ni–12.7 wt% Al) alloy ingot was prepared by conventional induction heating and homogenized at 1573 K for 36 ks in high vacuum. Then the ingot was scrapped with a planer machine, crushed to powders by mechanical milling, and sieved less than 150  $\mu\text{m}$  in size. The powder was dipped in a stirring 20 wt% NaOH aqueous solution at 340 K for 18 ks in order to leach aluminum. After leaching the NaOH solution was subjected to inductively coupled plasma (ICP) analysis in order to measure the amount of leached aluminum. Subsequently, the powder was filtered out and rinsed in deionized water until the washing water became neutral pH 7. Finally, it was dried at 323 K for 28.8 ks in air. The surface area of the powder was determined by BET (Brunauer–Emmett–Teller) surface area analysis. The crystal structure before and after leaching was analyzed by X-ray diffraction (XRD) using a Cu K $\alpha$  source (Rigaku, RINT2500). For comparison, a nickel catalyst was prepared by the same leaching treatment from commercial Ni–50 wt% Al alloy powder (Raney-Nickel, Mitsuwa Chemicals).

The catalytic experiments of hydrogen production from methanol were carried out in a conventional fixed-bed flow reactor as described in the previous report [16]. The Ni<sub>3</sub>Al powder of 0.2 g was set in a quartz tube with an internal diameter of 8 mm in the reactor. Prior to reaction, the powder was reduced at 513 K for 3.6 ks in a flowing hydrogen atmosphere. Then, the hydrogen flow was stopped and refilled with nitrogen to flush H<sub>2</sub>. Subsequently, the mixed solution of methanol and water (CH<sub>3</sub>OH:H<sub>2</sub>O=1 mol:1.5 mol) was introduced to the quartz tube at a liquid hourly space velocity of 30 h<sup>-1</sup> (defined as the volume of methanol passed over the unit volume of catalyst per hour) using a plunger pump together with nitrogen carrier gas. Finally, temperature was increased stepwise from 513 to 633 K at intervals of 20 K. The outlet composition of gas products was analyzed after 1.5 ks at each temperature using gas chromatograph (Shimadzu, GC-14B equipped with thermal conductivity detectors). The total flow rate of gas products was measured at each temperature with a soap bubble meter just after the gas analysis. After the catalytic experiments, the surface of the powder was observed by a scanning electron microscopy with a field emission gun (JEOL, JSM-6500F).

## 3. Results and discussion

### 3.1. Surface characterization

The ICP analysis of the NaOH solution after leaching showed that aluminum was selectively leached from the Ni<sub>3</sub>Al powder. The amount of leached aluminum was estimated at 13.9 wt% of aluminum concentration in the precursor Ni<sub>3</sub>Al (Ni–12.7 wt% Al). No nickel was detected

Table 1  
Results of BET surface area measurements (m<sup>2</sup>/g)

	Before leaching	After leaching	After reaction
Ni <sub>3</sub> Al	2.3	5.1	5.7
Ni catalyst	1.8	2.8	1.8

in the solution. In the case of the nickel catalyst, much larger amount of aluminum was leached in the same process as the Ni<sub>3</sub>Al. The amount of leached aluminum was estimated at 78.4 wt% of aluminum concentration in the precursor Ni–50 wt% Al alloy.

Table 1 summarized the results of the BET surface area measurement. It is found that the surface area increases more than twice by leaching. Fig. 1 shows the size distribution of the surface pore before and after leaching which is estimated from the BET measurement. The pore radius is sharply distributed at approximately 2 nm after leaching, indicating that the observed increase in surface area is due to the formation of these fine pores. For the nickel catalyst we used for comparison, the surface area after leaching, 2.8 m<sup>2</sup>/g, is smaller than that of the Ni<sub>3</sub>Al catalyst. This is ascribed to the fact that the nickel catalyst was dried in air. As well known, Raney nickel catalysts have large surface area above 40 m<sup>2</sup>/g after leaching [3]. Since they are very reactive in air they are usually processed in inert or reducing environment. Probably, the surface of the nickel catalyst was oxidized during the drying process, resulting in the reduction in surface area. However, the catalytic characteristics of the nickel catalyst are not qualitatively damaged by this process, which will be described below.

The XRD analysis was carried out for the Ni<sub>3</sub>Al (Fig. 2a) and Ni (Fig. 2b) catalysts before and after leaching. As shown in Fig. 2a, all the diffraction peaks observed are assigned as Ni<sub>3</sub>Al. No significant difference is observed between before and after leaching. On the other hand, as shown in Fig. 2b, the Raney-Nickel powder before leaching (Ni–50 wt%Al) is composed of Ni<sub>2</sub>Al<sub>3</sub> and NiAl<sub>3</sub>.

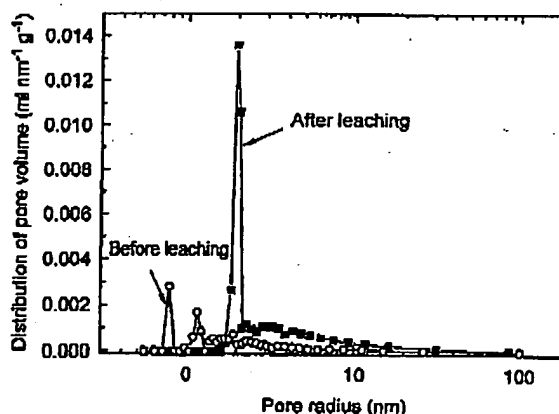


Fig. 1. Pore distribution in Ni<sub>3</sub>Al powder before and after leaching in 20 wt% NaOH at 340 K for 18 ks.

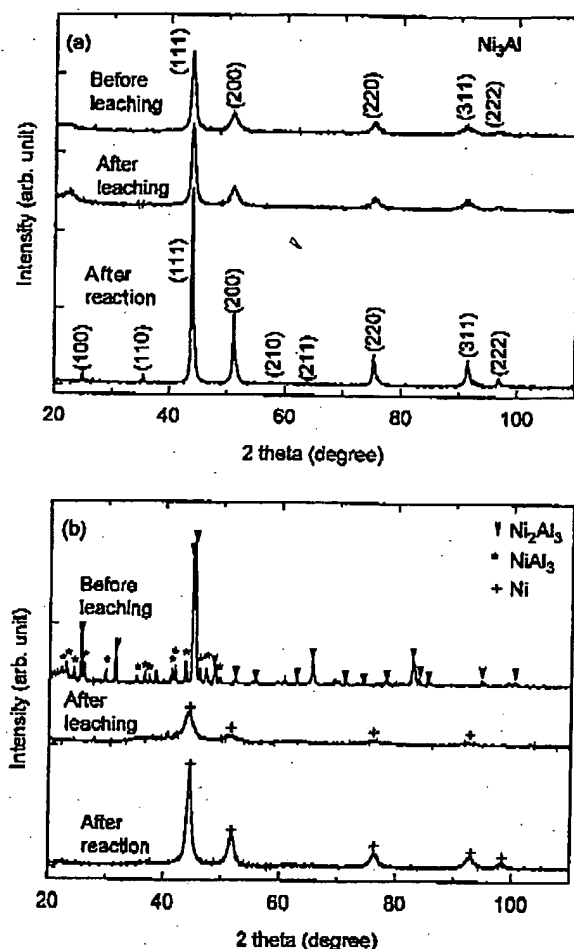


Fig. 2. XRD patterns of  $\text{Ni}_3\text{Al}$  (a) and Raney-nickel (b) powders before and after alkali leaching, and after catalytic reaction.

After leaching, the diffraction peaks of nickel are observed. Fig. 3 shows the SEM micrographs of the powder surface before and after leaching, showing no difference between them. Taking into account the fact that very fine pores (2 nm in radius) are formed by leaching (Fig. 1), the SEM observation is reasonable.

All the results indicate that leaching of aluminum is limited to the very thin surface layer of the  $\text{Ni}_3\text{Al}$  powder, leaving the bulk as it is. In the case of the nickel catalyst, f.c.c. Ni phase was formed on the surface as a result of alkali leaching.

### 3.2. Catalytic activity

The catalytic experiments of hydrogen production from a mixed solution of methanol and water were carried out. Fig. 4 shows the rates of  $\text{H}_2$ , CO,  $\text{CO}_2$  and  $\text{CH}_4$  productions as a function of the reaction temperature for the  $\text{Ni}_3\text{Al}$  before and after leaching. It is found that  $\text{H}_2$  and CO are the main products in the whole temperature range and that their

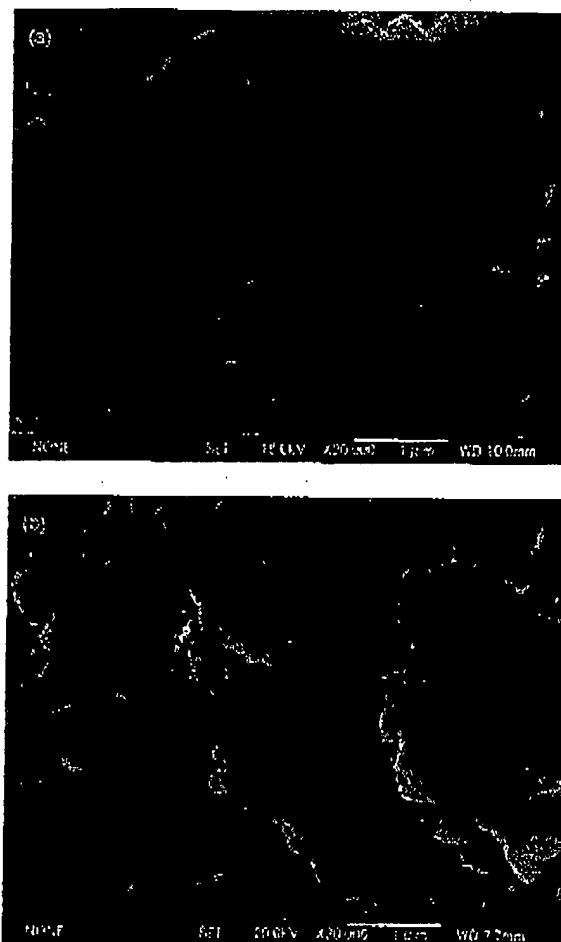


Fig. 3. SEM images of the surface of  $\text{Ni}_3\text{Al}$  powder: (a) before leaching, (b) after leaching.

production rate increases with increasing temperature for both the  $\text{Ni}_3\text{Al}$  catalysts. The results mean that water does not participate in the chemical reaction, i.e. the steam reforming of methanol ( $\text{CH}_3\text{OH} + \text{H}_2\text{O} \rightarrow 3\text{H}_2 + \text{CO}_2$ ) does not occur, the methanol decomposition mainly occurs in the presence of the  $\text{Ni}_3\text{Al}$  catalysts



The noteworthy in the results is threefold. First,  $\text{Ni}_3\text{Al}$  exhibits a limited catalytic activity without leaching. Second, the production rate of  $\text{H}_2$  and CO is much higher for the  $\text{Ni}_3\text{Al}$  after leaching than that before leaching, which means that the catalytic activity of  $\text{Ni}_3\text{Al}$  is markedly enhanced by leaching. Needless to say, the high production rate of hydrogen is beneficial to hydrogen production. Third, the production rate of  $\text{CO}_2$  and  $\text{CH}_4$  for the  $\text{Ni}_3\text{Al}$  before leaching is much lower in the whole temperature range, indicating high selectivity for methanol decomposition. Above 573 K the amounts of  $\text{CO}_2$  and  $\text{CH}_4$  increase slightly for the  $\text{Ni}_3\text{Al}$  after leaching. The following water gas shift

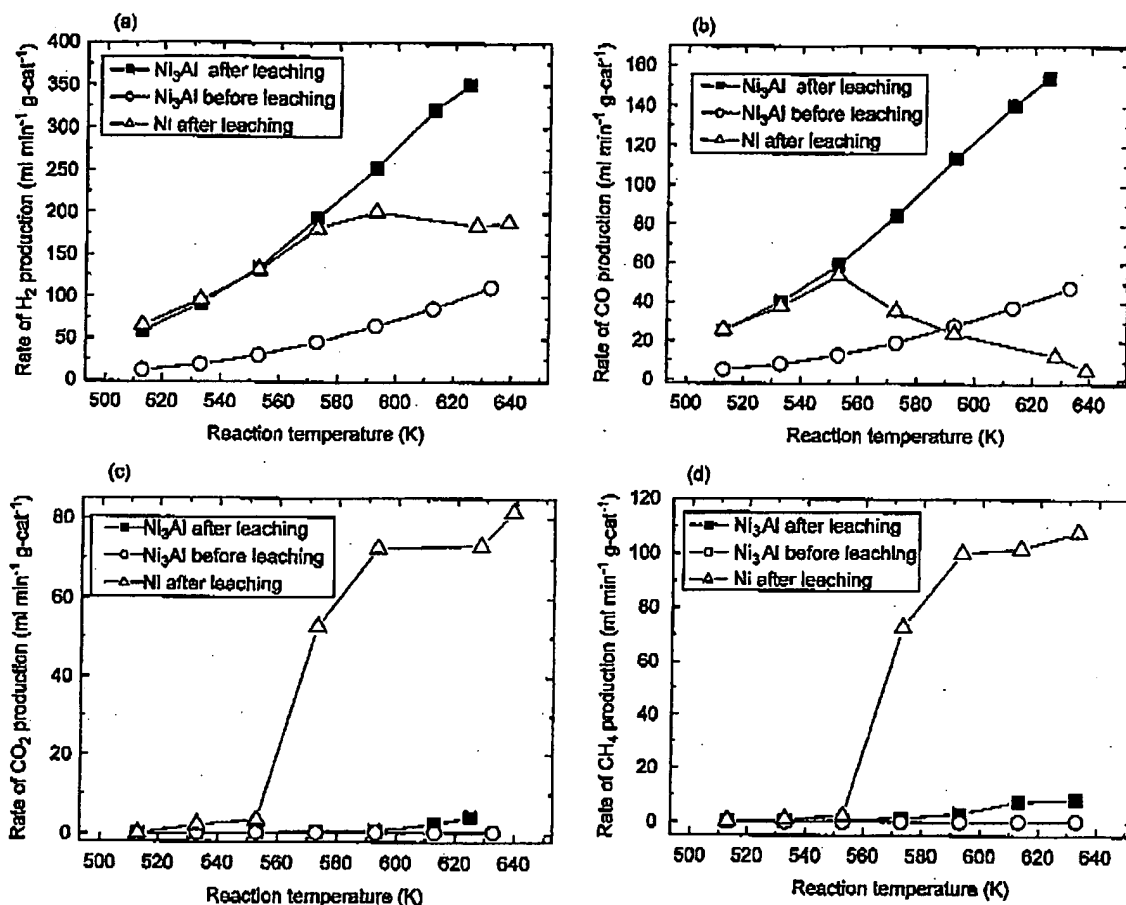
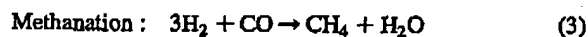


Fig. 4. The rate of (a) H<sub>2</sub>, (b) CO, (c) CO<sub>2</sub>, and (d) CH<sub>4</sub> productions at various reaction temperatures in the hydrogen production from methanol over the Ni<sub>3</sub>Al catalysts before leaching (circles), after leaching (squares), and over the nickel catalyst after leaching (triangles), respectively.

reaction and methanation, therefore, partly occur at high temperatures in addition to the methanol decomposition:



However, the production rate of methane is so small that the production rate of H<sub>2</sub> is not virtually affected in the temperature range of this study.

For comparison, the results of the nickel catalyst are also shown in Fig. 4. It is found that the nickel catalyst shows similar activity and selectivity for methanol decomposition below 553 K to the Ni<sub>3</sub>Al catalysts, while the water gas shift reaction and the methanation are highly accelerated above 553 K, accompanying the significant increase of CO<sub>2</sub> and CH<sub>4</sub> production rates. These results are qualitatively consistent with previous studies: the nickel catalysts are active for methanol decomposition [11,12], methanation [1,2,13], and water gas shift reaction [14,15]. As a result of the two concurrent reactions, the rate of H<sub>2</sub> production saturates above 590 K. The results demonstrate

the advantage of the Ni<sub>3</sub>Al catalysts over the nickel catalysts in terms of the selectivity for methanol decomposition at high temperatures above 553 K.

The XRD analysis of the Ni<sub>3</sub>Al powder after reaction was carried out and all the diffraction peaks were assigned as Ni<sub>3</sub>Al as shown in Fig. 2a, indicating that no structure change was observed during the catalytic reaction. The increase of the intensity of diffraction peaks after reaction is considered to be due to the strain annealing of the mechanically milled Ni<sub>3</sub>Al powder above 573 K. The BET surface area was measured at 5.7 m<sup>2</sup>/g, which is close to that of the Ni<sub>3</sub>Al after leaching as shown in Table 1. These results show that the Ni<sub>3</sub>Al catalysts have good thermal and chemical stabilities, which are considered to take over the excellent high temperature strength and corrosion/oxidation resistance of Ni<sub>3</sub>Al even after alkali leaching.

Considering that the Ni<sub>3</sub>Al before leaching shows a low catalytic activity, the high activity of the Ni<sub>3</sub>Al after leaching cannot be explained simply by the increase in surface area. The outer surface of the Ni<sub>3</sub>Al must become nickel-enriched after leaching and it is, therefore,

considered that the nickel-enriched surface, which may be a mixture of  $\text{Ni}_3\text{Al}$  and  $\text{Ni}$ , increases the catalytic activity and does not decrease the selectivity significantly for methanol decomposition, by suppressing methanation and water gas shift reaction. Detailed surface analysis is in progress.

#### 4. Conclusions

The catalytic activity of  $\text{Ni}_3\text{Al}$  before and after alkali leaching was studied for hydrogen production from methanol in the temperature range of 513–633 K. The following results were obtained. These results indicate that the  $\text{Ni}_3\text{Al}$  catalysts are highly promising as a catalyst for hydrogen production.

- (1)  $\text{Ni}_3\text{Al}$  single-phase alloy, i.e.  $\text{Ni}_3\text{Al}$  before alkali leaching, shows a limited catalytic activity for the methanol decomposition, and no activity for the steam reforming of methanol.
- (2) The activity of  $\text{Ni}_3\text{Al}$  for the methanol decomposition is improved significantly by alkali leaching. The alkali-leached  $\text{Ni}_3\text{Al}$  catalysts show a higher catalytic activity for the methanol decomposition than nickel catalyst above 573 K. The rate of hydrogen production increases rapidly with increasing reaction temperature. A rate of  $\text{H}_2$  production up to  $350 \text{ ml min}^{-1}$  per  $\text{g cat}^{-1}$  was obtained at 625 K.

- (3) The  $\text{Ni}_3\text{Al}$  catalysts suppress the formation of methane and water gas shift reaction, i.e. they show higher selectivity for methanol decomposition than nickel catalysts.

#### References

- [1] Mills GA, Steffen FW. *Catal Rev* 1973;8:159.
- [2] Vannice MA. *Catal Rev—Sci Eng* 1976;14:153.
- [3] Huber GW, Shabaker JW, Dumesic JA. *Science* 2003;300:2075.
- [4] Komatsu T, Hyodo S, Yashima T. *J Phys Chem B* 1997;101:5565.
- [5] Komatsu T, Fukui M, Yashima T. In: Hightower JW et al, editor. 11th International Congress on Catalysis—40th Anniversary Studies. *Surf. Sci. Catal.*, vol. 101. Amsterdam: Elsevier; 1996. p. 1095.
- [6] Tanaka S, Hirose N, Tanaki T, Ogata YH. *J Electrochem Soc* 2000; 147:2242.
- [7] Pope DP, Ezz SS. *Int Mater Rev* 1984;29:136.
- [8] Stoloff NS. *Int Mater Rev* 1989;34:153.
- [9] Yamaguchi M, Umakoshi Y. *Mater Sci* 1990;34:1.
- [10] Rostrup-Nielsen JR. *Phys Chem Chem Phys* 2001;3:283.
- [11] Yasumori I, Nakamura T, Miyazaki E. *Bull Chem Soc Jpn* 1967;40: 1372.
- [12] Chen B, Falconer JL. *J Catal* 1993;144:214.
- [13] Happel J, Suzuki I, Kokayeff P, Pthenakis V. *J Catal* 1980;65:59.
- [14] Grenoble DC, Estadt MM, Ollis DF. *J Catal* 1981;67:90.
- [15] Mizuno K, Yoshikawa K, Wakejima N. *Chem Soc Jpn, Chem Lett* 1986;1969.
- [16] Tsai AP, Yoshimura M. *Appl Catal, A: Gen* 2001;214:237.



## Spontaneous catalytic activation of $\text{Ni}_3\text{Al}$ thin foils in methanol decomposition

Dong Hyun Chun<sup>a,b,\*</sup>, Ya Xu<sup>b</sup>, Masahiko Demura<sup>b</sup>, Kyosuke Kishida<sup>c</sup>, Dang Moon Wee<sup>a</sup>,  
Toshiyuki Hirano<sup>b</sup>

<sup>a</sup> Department of Materials Science and Engineering, KAIST, Daejeon 305-701, South Korea

<sup>b</sup> National Institute for Materials Science, 1-2-1 Sengen, Tsukuba, Ibaraki 305-0047, Japan

<sup>c</sup> Department of Materials Science and Engineering, Kyoto University, Kyoto 606-8501, Japan

Received 13 May 2006; revised 28 June 2006; accepted 6 July 2006

Available online 22 August 2006

### Abstract

Methanol decomposition was carried out over flat cold-rolled foils of intermetallic compound  $\text{Ni}_3\text{Al}$  in a temperature range 513–793 K. The methanol decomposition into  $\text{H}_2$  and CO was effectively catalyzed at 713–793 K, without any need for coating catalyst layers on the foil surface before reaction. Both catalytic activity and selectivity to  $\text{H}_2$  and CO production increased with time during the initial period of reaction, indicating that the  $\text{Ni}_3\text{Al}$  foils were spontaneously activated under the reaction conditions. Analysis of the catalytic reaction revealed that the methanol decomposition accompanied three minor side reactions: the Boudouard reaction, (reverse) water–gas shift reaction, and methanation. Surface analyses revealed that fine Ni particles dispersed on carbon nanofibers formed on the  $\text{Ni}_3\text{Al}$  foils during the reaction at 713–793 K. We attribute the high catalytic performance at 713–793 K to the gradual formation of this nanostructure.  
© 2006 Elsevier Inc. All rights reserved.

**Keywords:** Intermetallic compounds and alloys; Microreactor; Methanol decomposition; Carbon nanofibers

### 1. Introduction

In recent years, microchanneled reactors have received much attention as compact and efficient hydrogen production systems utilizing alcohol or hydrocarbon, due to their high surface-to-volume ratio and high rates of heat and mass transfer compared with conventional reactors [1–9]. In many cases, stainless steel or silicon-based materials have been used as structural sheets, and active catalysts and porous support materials are coated on the structural sheets by complex chemical processes [1–6]. However, the lack of heat resistance in stainless steel and the poor formability and mechanical strength in silicon-based materials have limited the application range of microchanneled reactors. It is therefore necessary to develop new materials not only with high heat-resistance but also with good formability and mechanical strength. Furthermore, simplification of the

complex coating process of catalyst layers is considered as an important subject in microchanneled reactor technologies.

In this respect, intermetallic compound  $\text{Ni}_3\text{Al}$ , an excellent high-temperature structural material [10,11], has considerable promise. Thus far, we have successfully developed thin foils (23  $\mu\text{m}$ ) of this compound by cold-rolling [12]. Because the foils have good formability after proper heat treatment [13], they can be assembled into honeycomb monoliths [14] and microchanneled reactors [15]. In addition, we recently have found high catalytic activity and selectivity for methanol decomposition into  $\text{H}_2$  and CO in the foils [16,17]. The unusually high catalytic performance of the flat  $\text{Ni}_3\text{Al}$  foils is attributed to this catalytically active structure; that is, fine Ni particles supported on carbon nanofibers form spontaneously on the foil surface during the reaction. The results of previous studies [10–17] demonstrate that the  $\text{Ni}_3\text{Al}$  foils can be used both as catalysts and structural sheets of microchanneled reactors for hydrogen production from methanol.

In our previous study, we reported the catalytic properties for methanol decomposition at one specific temperature 793 K. In

\* Corresponding author. Fax: +82 42 869 4275.  
E-mail address: [cdhsl@kaist.ac.kr](mailto:cdhsl@kaist.ac.kr) (D.H. Chun).

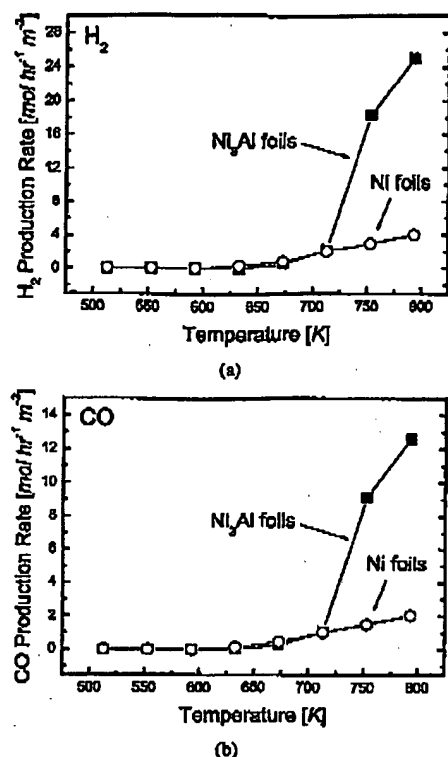


Fig. 1. Production rates of (a) H<sub>2</sub> and (b) CO in methanol decomposition over Ni<sub>3</sub>Al foils as a function of reaction temperature. For comparison, the result over Ni foils is inserted.

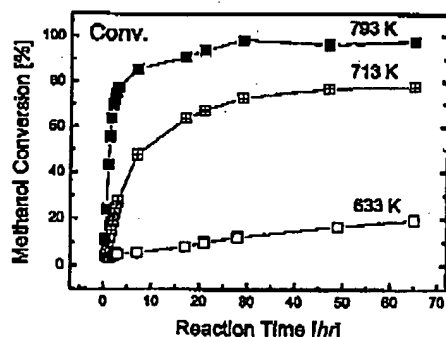
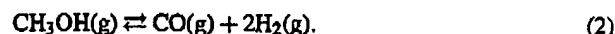


Fig. 2. Methanol conversion over Ni<sub>3</sub>Al foils at 633, 713, and 793 K as a function of reaction time.

increasing reaction time during the first several hours, reaching a steady-state value of about 98% after 29 h of reaction, as we previously reported [16]. No considerable change occurred thereafter. Methanol conversion showed a similar tendency at 713 and 633 K; however, both the initial increasing rate and the steady-state value were low at these temperatures compared with those at 793 K.

Fig. 3 shows the production rates of outlet gases as a function of reaction time, as we previously reported [17]. As shown in Figs. 3a and 3b, the production rates of H<sub>2</sub> and CO were much higher than those of other gases for all conditions, and thus the main reaction was



Both production rates increased with increased reaction time and temperature, corresponding to the methanol conversion, as shown in Fig. 2. This behavior is quite different from that of common Ni catalysts for methanol decomposition. For example, for Ni/SiO<sub>2</sub> catalysts, methanol initially decomposes into H<sub>2</sub> and CO, but methanation of CO soon follows via the consumption of H<sub>2</sub>. As a result, the main products are CH<sub>4</sub>, CO<sub>2</sub>, and H<sub>2</sub>O [20]. Fig. 4 shows that the ratio of both production rates is higher than the stoichiometric value of Eq. (2) at the initial reaction period (H<sub>2</sub>/CO = 2.0), and that it decreases to the stoichiometric value with increased reaction time.

Small amounts of H<sub>2</sub>O, CH<sub>4</sub>, and CO<sub>2</sub> were also produced along with the main products, as shown in Figs. 3c–3e. Note the difference in the vertical scale between Figs. 3c–3e and Figs. 3a–3b. The production rates of these minor products generally increased with increasing temperature and time, but the time dependence was different from that for methanol conversion, particularly at 793 K. The production rate of H<sub>2</sub>O increased rapidly with increased time at the beginning of the reaction (Fig. 3c), then decreased slightly and gradually increased again, showing a local maximum and minimum. In contrast, the production rates of CH<sub>4</sub> and CO<sub>2</sub> increased gradually and continuously with increased time even after the methanol conversion reached almost 100% (after 29 h). Nevertheless, the production rate of CH<sub>4</sub> was extremely low compared with that over Ni/SiO<sub>2</sub> catalysts. (CH<sub>4</sub> is the major product of methanol decomposition over Ni/SiO<sub>2</sub> catalysts [20].)

### 3.3. Surface characterization after isothermal tests

Before the reaction, the foil surface was macroscopically smooth with a shiny metallic luster, but had a rolling deformation structure [21]. After the isothermal tests at all reaction temperatures, the surface was covered in soot due to deposition of carbon during the reaction. Surface observation by SEM (Fig. 5) revealed a drastic evolution of reaction products during the reaction. At 793 K, small Ni particles (<250 nm in diameter) formed on the foil surface after 1 h of reaction (Fig. 5i). After 2 h of reaction, carbon nanofibers formed (Fig. 5j). Both the Ni particles and the carbon nanofibers were identified by TEM and XRD. The Ni particles were dispersed on the carbon nanofibers. The size of the particles corresponded closely with the diameter of the carbon nanofibers. The number of both products significantly increased over the entire surface of the foils with increasing reaction time (Figs. 5j–5l). After 7 h of reaction, most of the Ni particles were <100 nm in diameter, as we reported previously [16]. After 65 h of reaction, the particle size ranged from several tens to hundreds of nanometers in diameter. The particles <100 nm in diameter tended to be located at the top of the carbon nanofibers, and those >100 nm in diameter tended to be located on the middle region of the fibers. At 713 K, Ni particles also formed after 1 h of reaction (shown by arrows in Figs. 5e and 5f). However, the particles were sparsely distributed and small compared with those at 793 K. Blocky products were observed at this stage but remained unidentified.

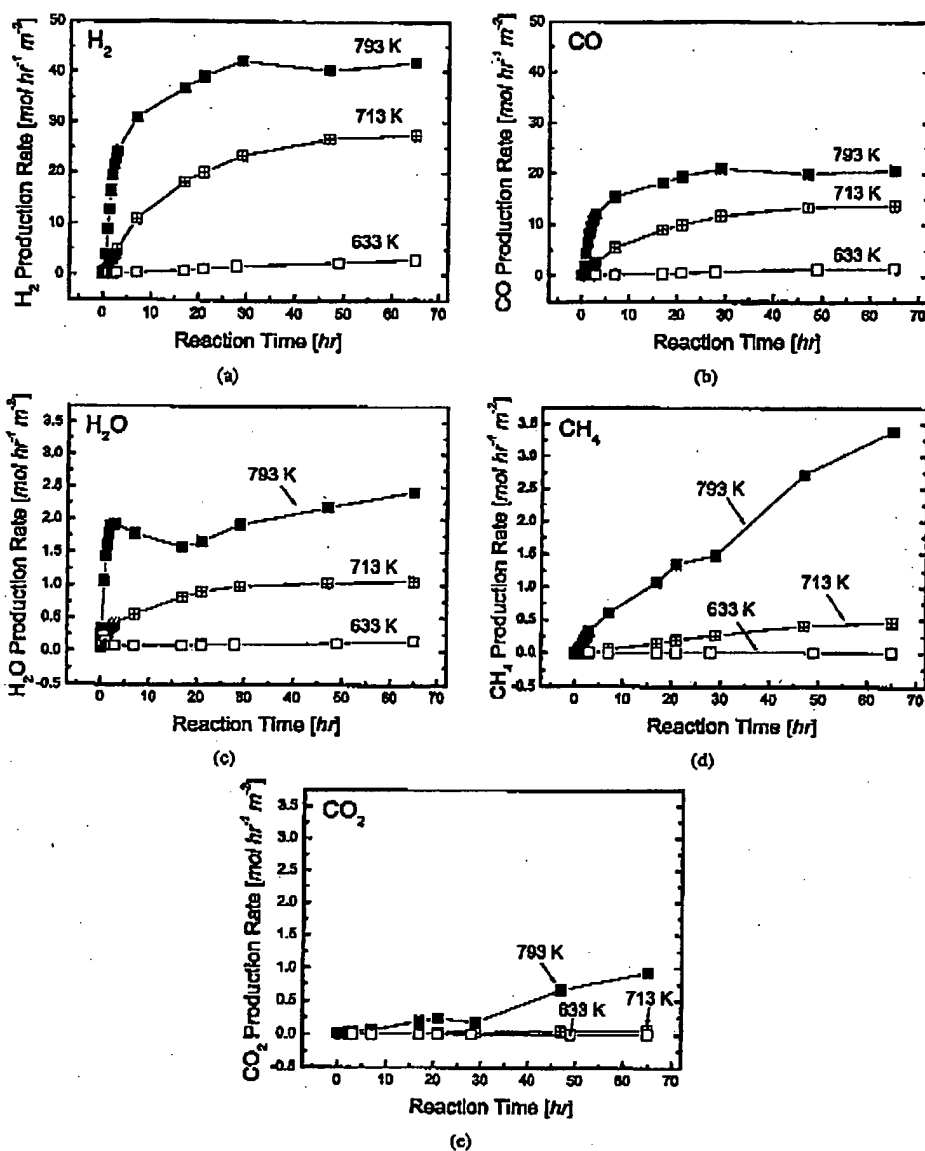


Fig. 3. Production rates of (a)  $\text{H}_2$ , (b) CO, (c)  $\text{H}_2\text{O}$ , (d)  $\text{CH}_4$ , and (e)  $\text{CO}_2$  in methanol decomposition over  $\text{Ni}_3\text{Al}$  foils at 633, 713, and 793 K as a function of reaction time.

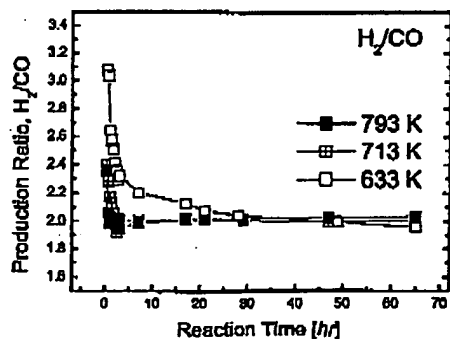


Fig. 4. Ratio of  $\text{H}_2$  to CO production in methanol decomposition over  $\text{Ni}_3\text{Al}$  foils at 633, 713, and 793 K as a function of reaction time.

Formation of carbon nanofibers was slow compared to that at 793 K; specifically, nanofibers formed after 7 h of reaction. After 65 h of reaction, there was no difference in the size and distribution of either the Ni particles or the carbon nanofibers between 713 and 793 K (Figs. 5h and 5i). At 633 K, formation of reaction products was quite slow. The amount of Ni particles was negligible until 7 h of reaction, and no carbon nanofiber was observed on the surface though the whole range of reaction time (Figs. 5a–5d).

A detailed surface structure analysis was performed on the foil after 1 h of reaction at 793 K (Fig. 5i) using TEM and STEM-EDS, as shown in Fig. 6. The cross-sectional TEM image shows the formation of a small particle and a thin layer on the foils. The elemental mapping by STEM-EDS revealed



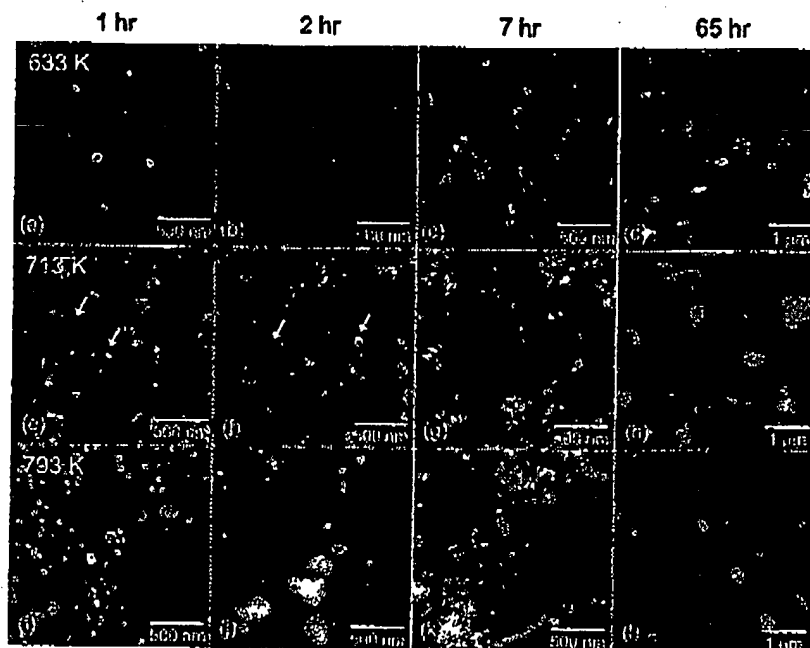


Fig. 5. Surface SEM images of  $\text{Ni}_3\text{Al}$  foils after (a, e, i) 1 h, (b, f, j) 2 h, (c, g, k) 7 h, and (d, h, l) 65 h of reaction at (a–d) 633 K, (e–h) 713 K, and (i–l) 793 K.

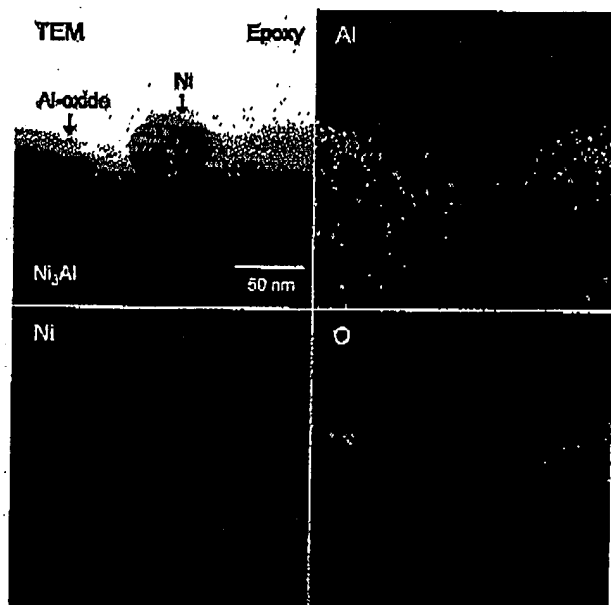


Fig. 6. Cross-sectional TEM image and corresponding elemental mapping by STEM-EDS for  $\text{Ni}_3\text{Al}$  foils after 1 h of reaction at 793 K.

that the particles contained mainly Ni and almost no Al and O, thus confirming the formation of small Ni particles on the surface at the beginning of the reaction. The thin layer contained mainly Al and O, indicating the formation of Al-oxide, which agrees well with our previously reported XPS results [16] that Al in the  $\text{Ni}_3\text{Al}$  foils was selectively oxidized and hydroxylated during methanol decomposition. As we previously discussed,

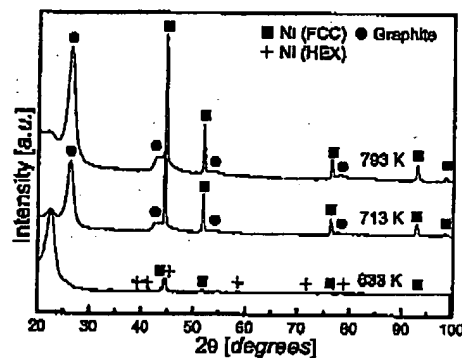


Fig. 7. XRD patterns for surface products on  $\text{Ni}_3\text{Al}$  foils after 65 h of reaction at 633, 713, and 793 K.

selective oxidation and/or hydroxylation of Al in the  $\text{Ni}_3\text{Al}$  foils is thought to leave Ni atoms behind, resulting in aggregation into small Ni particles. The small Ni particles can serve as effective catalysts for methanol decomposition.

The crystal structures of the surface products after 65 h of reaction were characterized by XRD, as shown in Fig. 7. The XRD patterns confirmed the formation of graphite and metallic Ni at 713 and 793 K, which are often reported in Ni particles supported on carbon nanofibers [22,23]. In contrast, the XRD patterns showed the formation of metallic Ni and no graphite at 633 K, indicating that the carbon produced was likely amorphous.

Surface areas of the samples before and after 65 h of reaction are given in Table 1. The surface area before reaction was approximately  $17 \text{ m}^2/\text{m}^2$ . Therefore, the BET surface area of the cold-rolled  $\text{Ni}_3\text{Al}$  foils is roughly 17 times greater than the geo-

Table 1  
Surface area ( $\text{m}^2/\text{m}^2$ ) of  $\text{Ni}_3\text{Al}$  foils before and after 65 h of reaction at 633, 713, and 793 K. The surface area was obtained by normalizing the BET surface area ( $\text{m}^2$ ) into the geometrical surface area ( $\text{m}^2$ )

Before reaction ( $\text{m}^2/\text{m}^2$ )	After 65 h of reaction ( $\text{m}^2/\text{m}^2$ )		
	633 K	713 K	793 K
16.6	245.6	1959.1	1711.3

metrical value, possibly due to the deformation structure. After reaction at 713 and 793 K, the surface area increased significantly, to about 1960 and 1710  $\text{m}^2/\text{m}^2$ , respectively; thus, the surface area was 118 and 104 times larger, respectively, than the value before the reaction. The remarkable increase in surface area after reaction at 713 and 793 K is clearly due to the formation of the surface products, consisting of small Ni particles and carbon nanofibers. Notably, the increase in surface area after the reaction at 633 K was small compared with that at 713 and 793 K.

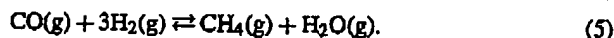
#### 4. Discussion

##### 4.1. Reaction system

In our previous studies, we reported the catalytic properties for methanol decomposition at one specific temperature, 793 K. In the present study, the temperature dependence of the catalytic properties became clear. The results reveal that methanol was largely decomposed into  $\text{H}_2$  and CO over cold-rolled  $\text{Ni}_3\text{Al}$  foils above 713 K, and that the amount of product gases increased with increased reaction time. Small amounts of  $\text{CH}_4$ ,  $\text{CO}_2$ ,  $\text{H}_2\text{O}$ , and solid-phase carbon were also produced as byproducts, but their production was significantly suppressed compared with that of common Ni catalysts. The results indicate that our reaction system cannot be described simply by the single stoichiometric reaction of Eq. (2). Several reactions must proceed simultaneously or consecutively. In this section, we discuss the possible mechanism in terms of catalytic reaction.

Selectivity of each reaction product in the reforming process of hydrocarbon has been calculated for the case without carbon deposition on the catalyst; that is, a complete carbon balance is obtained between the feed and effluent gases [24,25]. In our previous study, we neglected carbon deposition for the calculation of selectivity in the methanol decomposition over cold-rolled  $\text{Ni}_3\text{Al}$  foils [16]. However, a small amount of solid-phase carbon formed in the form of carbon nanofibers or amorphous carbon on the foil surface (Figs. 5 and 7). Thus, it is reasonable to take into account carbon deposition when calculating selectivity. However, measuring the production rate of carbon as a function of reaction time is not easy, and thus we alternatively estimated the rate based on the following assumption.

We propose the following three reactions proceed as side reactions in addition to the main reaction (Eq. (2)). Thus, the reaction system can be written as a combination of Eqs. (2)–(5):



Equations (3), (4), and (5) are referred to as Boudouard reaction, reverse water–gas shift reaction, and methanation, respectively.

Assuming the four stoichiometric reactions (Eqs. (2)–(5)), the production rate of carbon can be estimated simply by calculating the balance of the reactants and products as

$$R_{\text{C}} = R_{\text{CO}_2} + R_{\text{H}_2\text{O}} - R_{\text{CH}_4}, \quad (6)$$

where  $R_{\text{CO}_2}$ ,  $R_{\text{H}_2\text{O}}$ , and  $R_{\text{CH}_4}$  are the experimentally measured production rates of  $\text{CO}_2$ ,  $\text{H}_2\text{O}$ , and  $\text{CH}_4$ , respectively (Fig. 3). The detailed calculation procedure is described in Appendix A. Selectivities of  $\text{H}_2$  ( $S_{\text{H}_2}$ ) and the other carbon-containing reaction product, x, ( $S_x$ ) can be calculated from the production rates of the products according to Cortright et al. [25] as

$$S_{\text{H}_2} = \frac{R_{\text{H}_2}}{R_{\text{CO}} + R_{\text{CH}_4} + R_{\text{CO}_2} + R_{\text{C}}} \times \frac{1}{RR} \times 100, \quad (7)$$

$$S_x = \frac{R_x}{R_{\text{CO}} + R_{\text{CH}_4} + R_{\text{CO}_2} + R_{\text{C}}} \times 100, \quad (8)$$

where  $R_{\text{H}_2}$  is the experimentally measured production rate of  $\text{H}_2$  (Fig. 3) and  $RR$  is the  $\text{H}_2/\text{CO}$  ratio in Eq. (2); the  $RR$  value for methanol decomposition is 2.

Using Eqs. (7) and (8), the selectivities to  $\text{H}_2$  and CO production were calculated and plotted as a function of reaction time in Fig. 8. Both selectivities were low at the beginning of the reaction, particularly at the lower reaction temperatures. After the initial period, both selectivities increased with time, eventually reaching steady-state values of around 90% at all reaction temperatures. The increase of the selectivities was rapid at 713 K and above. At 793 K, both selectivities decreased slightly after 29 h of reaction when the methanol conversion reached almost 100%. However, they remained at high, >80%, even after 65 h of reaction. Our results confirm that methanol decomposition into  $\text{H}_2$  and CO (Eq. (2)) was the main reaction in the whole range of reaction temperatures and time in this study.

The selectivities to the production of minor components, C,  $\text{CH}_4$ , and  $\text{CO}_2$ , are shown in Fig. 9. The selectivity to C production was high at the beginning, particularly at lower temperatures, and decreased with time (Fig. 9a). At 793 K, selectivity to C production decreased to almost zero after 29 h of reaction when the methanol conversion reached almost 100%. This means that Boudouard reaction, as given in Eq. (3), occurred during the initial period of reaction. Occurrence of the Boudouard reaction may lead to the consumption of CO produced via the main reaction (Eq. (2)), resulting in a higher ratio of  $\text{H}_2$  to CO production than the stoichiometric value during the initial period of reaction (Fig. 4). In contrast, the selectivity to  $\text{CH}_4$  production increased gradually with increased reaction time, as shown in Fig. 9b, indicating that methanation (Eq. (5)) proceeded gradually over time. The selectivity to  $\text{CO}_2$  production in Fig. 9c showed a similar tendency to that of C production at the initial period, that is, rapid decrease with time. However, it again increased gradually at a later period.

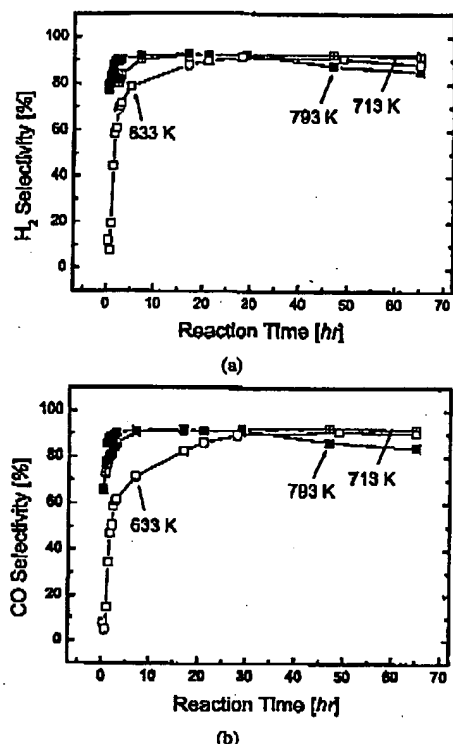


Fig. 8. Selectivities to (a) H<sub>2</sub> and (b) CO production in methanol decomposition over Ni<sub>3</sub>Al foils at 633, 713, and 793 K as a function of reaction time.

Considering that the selectivity of CO<sub>2</sub> was much lower than that of C in the initial period, CO<sub>2</sub> is likely produced via a Boudouard reaction (Eq. (3)) and consumed via a reverse water-gas shift reaction (Eq. (4)) at the initial period; that is, the initial period can be described by a combination of Eqs. (2), (3), and (4). On the other hand, because the selectivity to CO<sub>2</sub> production increased gradually at the later period, even after the Boudouard reaction (Eq. (3)) was terminated, the water-gas shift reaction (the reverse reaction of Eq. (4)) appears to have occurred with the progression of methanation (Eq. (5)) after the initial period. Thus, the reaction system at the later period can be described by a combination of Eqs. (2), (4), and (5). According to these considerations, the change in H<sub>2</sub>O production rate, as given in Fig. 3c, also can be adequately described.

Based on these analyses, we suggest that the methanol decomposition over cold-rolled Ni<sub>3</sub>Al foils proceeded mainly via the process described in Eq. (2), accompanying three minor side reactions (Eqs. (3)–(5)). Among the side reactions, the Boudouard reaction (Eq. (3)) and the reverse water-gas shift reaction (Eq. (4)) occurred preferentially during the initial period, and methanation (Eq. (5)) followed thereafter with the water-gas shift reaction (the reverse reaction of Eq. (4)).

#### 4.2. Activation process

As shown in Figs. 3 and 8, both the activity and the selectivity to H<sub>2</sub> production increased rapidly during the initial period

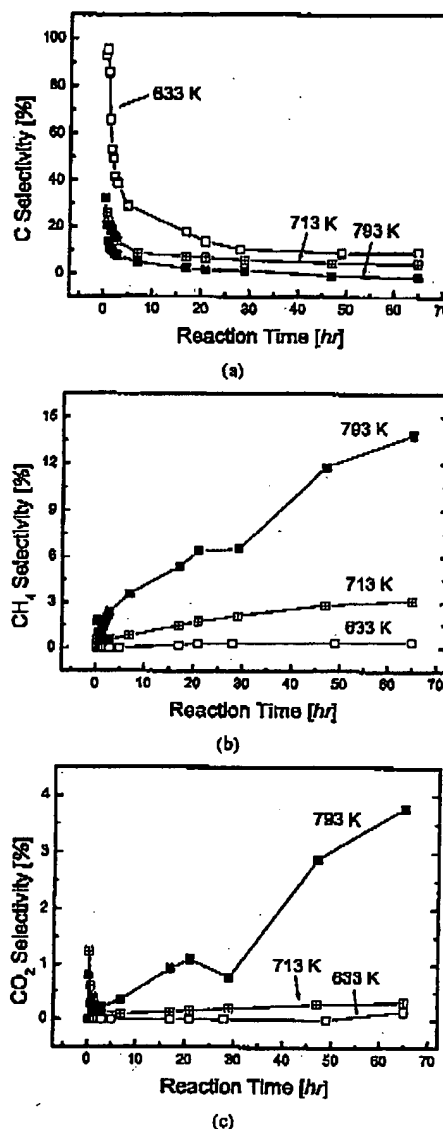
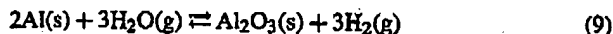


Fig. 9. Selectivities to (a) C, (b) CH<sub>4</sub>, and (c) CO<sub>2</sub> production in methanol decomposition over Ni<sub>3</sub>Al foils at 633, 713, and 793 K as a function of reaction time.

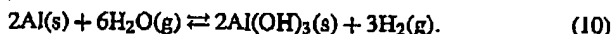
of reaction above 713 K. This rapid increase is favorable in terms of practical applications, demonstrating that efficient hydrogen production is possible using flat foils without the need for a complex coating process of the catalyst layers. In our previous study [16], we pointed out that the high catalytic activity can be attributed to the spontaneous formation of fine Ni particles dispersed on the carbon nanofibers.

Fine Ni particles are known to be active catalysts for methanol decomposition [20,26–30]. We consider this to hold true in the present study, as the increase in the number of Ni particles led to increased catalytic activity with increased reaction time. We have previously discussed the formation mechanism of fine Ni particles during the reaction based on the results of XPS analyses [16]; that is, Al in the Ni<sub>3</sub>Al foils is selectively

oxidized and hydroxylated to form  $\text{Al}_2\text{O}_3$  and  $\text{Al}(\text{OH})_3$  during the initial period of reaction. This oxidation mechanism may involve the following reactions:



and



The selective oxidation and hydroxylation of Al can lead to the formation of fine Ni particles, possibly because Ni atoms remain and aggregate into fine Ni particles. In this study, we confirmed by TEM observation that fine Ni particles and Al-oxide formed at the beginning of the reaction (Fig. 6). Considering that  $\text{H}_2$  and CO were the major products, the reaction atmosphere must have been highly reducing. However, because a small amount of  $\text{H}_2\text{O}$  was also produced via the reverse water-gas shift reaction (Eq. (4)) and/or methanation (Eq. (5), Fig. 3c), the oxygen partial pressure in the reaction atmosphere is considered low, in the range where  $\text{Al}_2\text{O}_3$  and  $\text{Al}(\text{OH})_3$  can form selectively. The observation that fine Ni particles were favorably produced at 713 K and above (Fig. 5) indicates that this mechanism works effectively at high temperatures. Several researchers have reported a similar mechanism for the oxidation of  $\text{Ni}_3\text{Al}$  under low oxygen partial pressures [31–33]. They found that pure metallic Ni particles and  $\text{Al}_2\text{O}_3$  formed above 773 K as a result of selective oxidation of Al in  $\text{Ni}_3\text{Al}$ , which is basically consistent with the mechanism described in the present study.

Carbon nanofibers are effective potential catalyst supports because of their high surface area with a large number of edges [34]. This characteristic surface is favorable for high catalytic performance because fine catalyst particles can be highly dispersed on the surface. Normally, carbon nanofibers are produced by the catalytic decomposition of hydrocarbon gases or carbon monoxide over selected metal particles, such as Fe, Co, and Ni, in a temperature range 673–1273 K [35,36]. In particular, in the temperature range 773–873 K, carbon nanofibers are more favorably produced over other types of carbon deposits, such as amorphous or graphitic carbons. In this study, carbon nanofibers formed above 713 K and amorphous carbon formed below 713 K (Figs. 5 and 7), which is consistent with previous reports [35,36]. The manner of carbon deposition is coincident with the formation of fine Ni particles; fine Ni particles formed densely above 713 K on the surface of carbon nanofibers.

We consider the formation of fine Ni particles and carbon nanofibers a coupled phenomenon, as illustrated in Fig. 10. First, fine Ni particles form as a result of selective oxidation and hydroxylation of Al, as described above. Then, formation of solid-phase carbon proceeds over the Ni particles via the Boudouard reaction (Eq. (3)). The deposited carbon possibly diffuses to grow in the form of a fibrous structure above 713 K, maintaining Ni particle surfaces that are free of deposited carbon, as previously proposed [35,36]. The produced carbon nanofibers are considered to suppress the coalescence of the Ni particles, acting as a means of support for heterogeneous catalysts [22,23,34]. These mechanisms may contribute

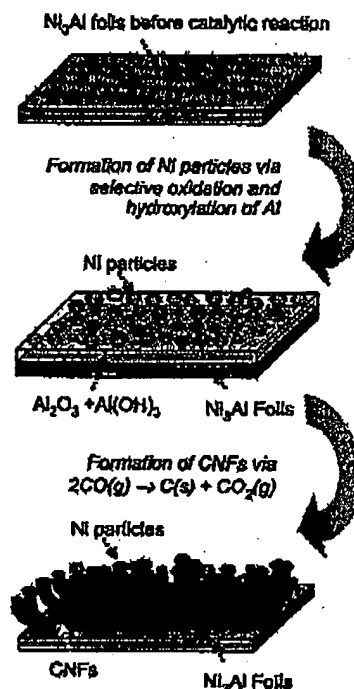


Fig. 10. Schematic diagram for spontaneous activation process of  $\text{Ni}_3\text{Al}$  foils during the reaction at 713–793 K.

to maintaining the catalytic activity and selectivity of the Ni particles during the reaction.

## 5. Conclusion

Catalytic properties of intermetallic compound  $\text{Ni}_3\text{Al}$  foils for methanol decomposition were evaluated at various reaction temperatures ranging from 513 to 793 K. Our main results can be summarized as follows:

- (1)  $\text{Ni}_3\text{Al}$  foils demonstrated high catalytic activity for methanol decomposition into  $\text{H}_2$  and CO in a temperature range 713–793 K but low catalytic activity below 713 K.
- (2) Both the catalytic activity and selectivity to  $\text{H}_2$  and CO production increased with increasing time during the initial period of reaction and became stable during the subsequent reaction.
- (3) The main reaction, methanol decomposition into  $\text{H}_2$  and CO (Eq. (2)), accompanied three minor side reactions: the Boudouard reaction (Eq. (3)), the reverse water-gas shift reaction (Eq. (4)), and methanation (Eq. (5)). Among the side reactions, the process described in Eqs. (3) and (4) occurred preferentially during the initial period, and that of Eq. (5) followed thereafter, accompanying the reverse reaction of Eq. (4).
- (4) Fine Ni particles dispersed on carbon nanofibers formed spontaneously on the foil surface at 713 K and above during the reaction. The rapid increase in the catalytic activity with increased time at 713–793 K is attributed to the spontaneous formation of this nanostructure.

## Acknowledgments

This work was supported in part by the Korea Science and Engineering Foundation (KOSEF-R01-2003-000-10433-0), the Korea Research Foundation Grant funded by the Korean government (MOBHD) (KRF-2005-213-D00038), and the Iketani Science and Technology Foundation, Japan.

## Appendix A

We estimated the production rate of solid-phase carbon by calculating the balance of the reactants and products appearing in three reactions (Eqs. (3)–(5)). The detailed procedures are as follows:

First, we assume that

$$R_{CO_2(Eq. (3))} = R_{C(Eq. (3))} = R_{C(total)}, \quad (A.1)$$

where  $R_{CO_2(Eq. (3))}$  and  $R_{C(Eq. (3))}$  are the production rates of  $CO_2$  and C via Eq. (3), respectively, and  $R_{C(total)}$  is the total production rate of C (estimated value). In the same way, we assume that

$$R_{CO_2(Eq. (4))} = R_{H_2O(Eq. (4))} = R_{H_2O(total)} - R_{H_2O(Eq. (5))}, \quad (A.2)$$

where  $R_{CO_2(Eq. (4))}$  and  $R_{H_2O(Eq. (4))}$  are the consuming rate of  $CO_2$  and the production rate of  $H_2O$  via Eq. (4), respectively,  $R_{H_2O(total)}$  is the total production rate of  $H_2O$  (measured value), and  $R_{H_2O(Eq. (5))}$  is the production rate of  $H_2O$  via Eq. (5). Also, we assume that

$$R_{CH_4(Eq. (5))} = R_{H_2O(Eq. (5))} = R_{CH_4(total)}, \quad (A.3)$$

where  $R_{CH_4(Eq. (5))}$  is the production rate of  $CH_4$  via Eq. (5) and  $R_{CH_4(total)}$  is the total production rate of  $CH_4$  (measured value). Furthermore, we assume that

$$R_{CO_2(total)} = R_{CO_2(Eq. (3))} - R_{CO_2(Eq. (4))} \quad (A.4)$$

from Eqs. (3) and (4), where  $R_{CO_2(total)}$  is the total production rate of  $CO_2$  (measured value). Finally, we can derive the total production rate of C as a function of the total production rates of  $CO_2$ ,  $H_2O$ , and  $CH_4$  from Eqs. (A.1)–(A.4) as

$$R_{C(total)} = R_{CO_2(total)} + R_{H_2O(total)} - R_{CH_4(total)}. \quad (A.5)$$

## References

- [1] M.T. Janicke, H. Kestenbaum, U. Hagendorf, F. Schürb, M. Fichtner, K. Schubert, *J. Catal.* 191 (2000) 282.
- [2] X. Yu, S.T. Tu, Z. Wang, Y. Qi, *Chem. Eng. J.* 116 (2006) 123.
- [3] J.Y. Won, H.K. Jun, M.K. Jeon, S.I. Woo, *Catal. Today* 111 (2006) 158.
- [4] Y. Kawamura, N. Ogura, T. Yamamoto, A. Igamshi, *Chem. Eng. Sci.* 61 (2006) 1092.
- [5] R.M. Tiggelaar, P.W.H. Loeters, P. Male, R.E. Oosterbroek, J.G.E. Gardniers, M.H.J.M. Croon, J.C. Schouten, M.C. Elwenspoek, A. Berg, *Sens. Actu. A Phys.* 112 (2004) 267.
- [6] R.M. Tiggelaar, P. Male, J.W. Berenschot, J.G.E. Gardniers, R.E. Oosterbroek, M.H.J.M. Croon, J.C. Schouten, A. Berg, M.C. Elwenspoek, *Sens. Actu. A Phys.* 119 (2005) 196.
- [7] A.S. Bodke, S.S. Bharadwaj, L.D. Schmidt, *J. Catal.* 179 (1998) 138.
- [8] I. Aartun, H.J. Vervik, A. Holmen, P. Pfeifer, O. Gürke, K. Schubert, *Catal. Today* 110 (2005) 98.
- [9] B.C. Wanaat, B. Suman, L.D. Schmidt, *J. Catal.* 235 (2005) 18.
- [10] N.S. Stoloff, C.T. Liu, S.C. Deevi, *Intermetallics* 8 (2000) 1313.
- [11] N.S. Stoloff, *Int. Mater. Rev.* 34 (1989) 153.
- [12] M. Demura, K. Kishida, Y. Suga, M. Takanashi, T. Hirano, *Scr. Mater.* 47 (2002) 267.
- [13] C. Cui, M. Demura, K. Kishida, T. Hirano, *J. Mater. Res.* 20 (2005) 1054.
- [14] K. Kishida, M. Demura, S. Kobayashi, Y. Xu, T. Hirano, *Defect. Diffus. Forum* 233–234 (2004) 37.
- [15] B.K. Paul, H. Hasan, T. Dewey, D. Almaz, R.D. Wilson, in: C. Mavroidis, P.S. Shiskolas, C.A. Moore, N. Sarkar, J.E. Speich (Eds.), *Proc. IMECE 2002, New Orleans, Louisiana, 17–22 November, 2002*, ASME, New York, 2002, pp. 32,892–32,897.
- [16] D.H. Chun, Y. Xu, M. Demura, K. Kishida, M.H. Oh, T. Hirano, D.M. Wee, *Catal. Lett.* 106 (2006) 71.
- [17] D.H. Chun, Y. Xu, M. Demura, K. Kishida, M.C. Kim, M.H. Oh, T. Hirano, D.M. Wee, *J. Kor. Inst. Met. Mater.* 43 (2005) 801.
- [18] Y. Xu, S. Kameoka, K. Kishida, M. Demura, A.P. Tsai, T. Hirano, *Intermetallics* 13 (2005) 151.
- [19] Y. Xu, S. Kameoka, K. Kishida, M. Demura, A.P. Tsai, T. Hirano, *Mater. Trans.* 45 (2004) 3177.
- [20] P.K. de Bokx, A.R. Balkende, J.W. Geus, *J. Catal.* 117 (1989) 467.
- [21] K. Kishida, M. Demura, T. Hirano, Y. Suga, in: S. Hanada, Z. Zhong, S.W. Nam, R.N. Wright (Eds.), *Proc. PRICM4, Hawaii, Honolulu, 11–15 December, 2001, JIM, Sendai, 2001*, pp. 867–870.
- [22] K. Otsuka, H. Ogihara, S. Takenaka, *Carbon* 41 (2003) 223.
- [23] S. Takenaka, E. Kato, Y. Tomikubo, K. Otsuka, *J. Catal.* 219 (2003) 176.
- [24] G.W. Huber, J.W. Shabaker, J.A. Dumesic, *Science* 300 (2003) 2075.
- [25] R.D. Cortright, R.R. Davda, J.A. Dumesic, *Nature* 418 (2002) 964.
- [26] A.R. Balkende, P.K. de Bokx, J.W. Geus, *Appl. Catal.* 30 (1987) 47.
- [27] K. Nakagawa, T. Hashida, C. Kajita, N. Ikenaga, T. Kobayashi, M. Nishitani-Gamo, T. Suzuki, T. Ando, *Catal. Lett.* 80 (2002) 161.
- [28] Y. Matsumura, N. Tode, T. Yazawa, M. Haruta, *J. Mol. Catal. A Chem.* 99 (1995) 183.
- [29] Y. Matsumura, K. Kuraoka, T. Yazawa, M. Haruta, *Catal. Today* 45 (1998) 191.
- [30] Y. Matsumura, K. Tanaka, N. Tode, T. Yazawa, M. Haruta, *J. Mol. Catal. A Chem.* 152 (2000) 157.
- [31] M. Haedig, S. Hofmann, *Appl. Surf. Sci.* 125 (1998) 99.
- [32] E. Schumann, G. Schnotz, K.P. Trumble, M. Rühle, *Acta Met. Mater.* 40 (1992) 1311.
- [33] W. Gao, Z. Li, Z. Wu, S. Li, Y. He, *Intermetallics* 10 (2002) 263.
- [34] N.M. Rodriguez, M.S. Kim, R.T.K. Baker, *J. Phys. Chem.* 98 (1994) 13,108.
- [35] R.T.K. Baker, *Encyclopedia of Materials: Science and Technology*, Elsevier, St. Louis, 1999, pp. 932–941.
- [36] R.T.K. Baker, *Am. Chem. Soc. Fuel Chem.* 41 (2) (1996) 521.